Title: TCR-ligand dissociation rate is a robust and stable biomarker of CD8+ T cell potency.

Authors: Allard M, Couturaud B, Carretero-Iglesia L, Duong MN, Schmidt J, Monnot GC, Romero P, Speiser DE, Hebeisen M, Rufer N

Journal: JCI insight

Year: 2017 Jul 20

Volume: 2

Issue: 14

DOI: 10.1172/jci.insight.92570

TCR-ligand dissociation rate is a robust and stable biomarker of CD8 T cell potency

Mathilde Allard[1], Barbara Couturaud[1], Laura Carretero-Iglesia[1], Minh Ngoc Duong[1], Julien Schmidt[2], Gwennaëlle Monnot[2], Pedro Romero[2], Daniel E. Speiser[1,2], Michael Hebeisen[1] and Nathalie Rufer[1,2]

[1]Department of Oncology, Lausanne University Hospital Center (CHUV) and University of Lausanne, Epalinges, Switzerland

[2]Ludwig Cancer Research, University of Lausanne, Epalinges, Switzerland

Conflict of interest statement: The authors have declared that no conflict of interest exists.

Address correspondence to:

Nathalie Rufer, PhD, MD, Department of Oncology, Lausanne University Hospital (CHUV), Biopôle 3 - 02DB92, chemin des Boveresses 155, CH-1066 Epalinges, Switzerland. Phone: +41 21 692.59.77. Fax: + 41 21 692 59 95. E-mails: Nathalie.Rufer@unil.ch

Running title: Identification of CD8 T cells with superior functional efficacy

Keywords: Human, CD8, T cells, melanoma, tumor-specific, virus-specific, TCR-pMHC off-rates, cytotoxicity, proliferation, cytokine production, activating/inhibitory receptor modulation, functional avidity, polyfunctionality

Abbreviations: HD; healthy donor, CMV; cytomegalovirus; EBV; Epstein-Barr virus, TCR; T cell receptor, EM; effector-memory, IFNγ; interferon-gamma; TNFα, tumor-necrosis factor

ABSTRACT

Despite influencing many aspects of T cell biology, the kinetics of T cell receptor (TCR) binding to peptide-major histocompatibility molecules (pMHC) remain infrequently determined in patient monitoring or for adoptive T cell therapy. Using specifically designed reversible fluorescent pMHC multimeric complexes, we performed a comprehensive study of TCR-pMHC off-rates combined with various functional assays on large libraries of self/tumor- and virus-specific CD8 T cell clones from melanoma patients and healthy donors. We demonstrate that monomeric TCR-pMHC dissociation rates accurately predict the extent of cytotoxicity, cytokine production, polyfunctionality, cell proliferation, activating/inhibitory receptor expression and in vivo anti-tumor potency of naturally occurring antigen-specific CD8 T cells. Our data also confirm the superior binding avidities of virus-specific T cells as compared to self/tumor-specific T cell clonotypes ($n > 300$). Importantly, the TCR-pMHC off-rate is a more stable and robust biomarker of CD8 T cell potency, than the frequently used functional assays/metrics that depend on the T cell's activation state and therefore show major intra- and inter-experimental variability. Together, the monomeric TCR-pMHC off-rate is highly useful for the ex vivo high throughput functional assessment of antigen-specific CD8 T cell responses and a strong candidate as a biomarker of T cell therapeutic efficacy.

INTRODUCTION

Cytotoxic T lymphocytes mediate immune protection against a large number of infectious diseases, and recent developments in oncology confirmed their ability to eliminate cancers. To achieve successful immunity, T cells must be activated through specific interactions between T cell receptors (TCR) and antigenic peptides presented by major histocompatibility molecules (pMHC) on antigen-presenting cells. This enables T cell expansion and differentiation into large numbers of effector cells with various functional capacities (i.e. killing, cytokine production, proliferation). Furthermore, T cells must migrate and localize to the infected or tumoral tissues, exerting their effector function and finally acquire memory properties, assuring long-lasting immunity.

Extensive research has been undertaken to determine which T cell properties are essential to generate protective and durable immune responses. T cell functional avidity, which measures in vitro T cell responses when exposed to increasing antigen concentrations, has been largely associated with the control of viral (1-3) or tumor (4, 5) load in animal models. In accordance with these observations, several findings in patients with HIV (6, 7) or hepatitis C (8, 9) infections further showed the key role of CD8 T cells of high functional avidity in efficient viral control and clearance. Yet, others have challenged the functional superiority of such high-avidity cells, which may be prone to increased activation-induced cell death, senescence or exhaustion (reviewed in (10)). In the context of anti-tumor responses, results obtained from melanoma patients also indicate that T cells of high functional avidities are required for efficient protection (11-13). Besides functional avidity, higher proportions of polyfunctional CD8 or CD4 T cells were also found in HIV (14, 15) and hepatitis C (16) controllers, when compared to individuals with progressive disease. Moreover, some reports proposed a direct link between functional avidity (i.e. antigen sensitivity) and polyfunctionality (i.e. T cell capacity to exert multiple effector functions) (17, 18). However, the ex vivo appraisal of T

cell functionality/polyfunctionality is still often limited to assays of fixed stimulation doses and by the lack of universal standards of T cell assessment (reviewed in (19, 20)). It is therefore essential to improve our knowledge regarding the contribution of the different aspects of T cell function to clinical efficacy and to identify additional T cell-based parameters that may enable overcoming some of the limitations associated to functional assays.

The functional avidity of T cells is primarily controlled by the strength of TCR-pMHC interactions, a key parameter shown to impact on numerous aspects of T cell biology, including their thymic selection (21), activation and differentiation (22), autoimmune pathogenicity (23), and protection against infection and cancer (24). In fact, TCR-pMHC binding avidity may offer a key metric by which the quality of the T cell response can be directly evaluated, since it controls T cell activation, differentiation and functional efficacy (25). Numerous studies indicate, that within the affinity range of physiological interactions (K_D 100 - 1 μM), enhanced TCR-pMHC affinity or off-rate (k_{off}) correlate with improved T cell functionality (26). However, most of these reports are based on artificial models (e.g. using affinity-optimized TCR variant panels or altered peptide ligand models), and thus only limited information is available on the overall impact and clinical relevance of TCR-pMHC binding avidity or kinetics (e.g. off-rates) in the context of naturally occurring antigen-specific CD8 T cell responses. Moreover, identifying and selecting TCRs of higher avidity may be of particular importance in the tumoral setting, since most high avidity/affinity self/tumor antigen-reactive T cells are naturally eliminated or silenced by mechanisms of central and peripheral tolerance, emphasizing the need to select the remaining rare high avidity cells for immunotherapy.

Reversible two-color multimer-based approaches (i.e. *Strep*tamers, NTAmers) have been developed to precisely quantify monomeric TCR-pMHC dissociation rates (i.e. off-rate or k_{off}) directly on living T cells. *Strept*amers initially revealed that virus-specific CD8 T cells with longer off-rates conferred better in vivo protection than T cells with shorter off-rates (27). However, owing to the faster decay of the multimeric complex onto monomeric pMHC when compared with *Strep*tamers, NTAmers offer an increased sensitivity to detect T cells of low avidity TCRs (26), such as those typically found in self/tumor-specific CD8 T cell repertoires. Consequently, we recently showed that NTAmer-based k_{off} strongly correlated with the killing capacity of TCR-engineered and natural tumor-specific human CD8 T cells (28, 29).

With the aim to thoroughly evaluate possible correlations between T cell function and TCR-pMHC binding kinetics, we here undertook a large-scale analysis of combined multiple functions (i.e. killing, CD107a degranulation, cytokine production, proliferation, surface expression of activating/inhibitory receptors and tumor control) and optimized off-rate measurements using NTAmers to characterize large libraries of tumor- and virus-specific CD8 T-cell clones isolated from melanoma patients and healthy donors. Our large data sets show that the TCR-pMHC off-rate is a major determinant controlling the functions of CD8 T cells in vitro and in vivo. Our findings are also of practical importance, as we found that the TCR-ligand dissociation rate is a highly stable biomarker, more reliable and reproducible than the usual assessments based on multimer staining levels or functional T cell avidity, which may fluctuate depending on the T cell's activation state.

RESULTS

TCR-pMHC off-rate accurately correlates to overall T cell functional avidity

To precisely address the relationship between the TCR-pMHC off-rate and the overall CD8 T cell functional profile, we generated large libraries of HLA-A*0201-restricted CD8 T cell clones, by direct ex vivo sorting and cloning of self/tumor-specific (i.e. Melan-A_{26-35} and NY-ESO-$1_{157-165}$) and virus-specific (i.e. Cytomegalovirus CMV/$pp65_{495-504}$ and Epstein-Barr virus EBV/$BMFL1_{259-267}$) effector-memory (EM) T cells (**Supplemental Figure 1**). We analyzed all clones for TCR-pMHC dissociation rates using NTAmers loaded with the native Melan-A, NY-ESO-1, EBV/BMFL1 or CMV/pp65 peptide because they provided a more physiological assessment of the TCR-pMHC recognition efficacy as opposed to the corresponding analog peptides (as detailed in Methods). Representative k_{off}-based panels of self/tumor- and virus-specific CD8 T cell clones were further characterized at the functional level, including assessment of cytotoxic activity, CD107a degranulation, and production of cytokines based on peptide titration assays, as well as proliferation (**Supplemental Figure 2**). Note that, for the same antigen-specificity, most of the different functional readouts/measures were obtained during the same non-specific restimulation cycle to make use of the antigen-specific CD8 T cell clones in a similar resting state (>D15 post restimulation).

We observed, for all antigenic specificities, statistically significant correlations between TCR-pMHC off-rates and various functional avidity readouts (EC_{50}, defined as the peptide concentration producing half-maximal response) or proliferative capacity (% of divided cells) (**Figure 1** and **Supplemental Figure 3, A and B**). Yet, stronger correlations ($p < 0.01$-0.001, $r > 0.5$ and narrow confidential intervals) were generally found for self/tumor- (Melan-A and NY-ESO-1) than non-self/virus- (CMV/pp65 and EBV/BMFL1) specific T cells. By contrast, no positive correlations could be observed between TCR-pMHC off-rates and the maximally

reached functions at saturating peptide doses (B_{max}, maximal response) (**Supplemental Figure 3C;** data not shown). In turn, the maximal response depended on the in vivo differentiation status, with stronger Th2-related cytokine production by clones derived from the early-differentiated EM/CD28$^+$ cells and greater granzyme B expression and killing by those from the late-differentiated EM/CD28$^-$ cells (**Supplemental Figure 3D)**. Collectively, these results indicate that, within an antigen-specific repertoire, the kinetics of TCR-pMHC interactions represent a major determinant of the overall functional avidity of CD8 T cells, regardless of their differentiation status (**Supplemental Figure 3D**) or function-specific activation thresholds (killing < CD107a < interferon-gamma (IFNγ) < tumor-necrosis factor alpha (TNFα) < IL-2) (**Supplemental Figure 4A**).

TCR-pMHC off-rate closely correlates to CD8 T cell polyfunctionality

Protective immunity against intracellular pathogens relies on the individual CD8 T cell capacity to display multiple effector functions or polyfunctionality (10). We hypothesized that the kinetics of TCR-pMHC interactions could also affect their polyfunctionality. The co-expression levels of CD107a, IFNγ, TNFα and IL-2 were characterized on a representative selection of self/tumor- and virus-specific CD8 T cell clones with relative slow or fast TCR-pMHC off-rates (**Figure 2**). For all antigenic specificities and peptide titrations tested, the fraction of cells displaying more than one single function was always greater in CD8 T cell clones with slower TCR-pMHC off-rates than with faster ones (**Figure 2A**). In line with these observations, we found that a significant proportion of antigen-specific CD8 T cell clones with slow TCR-pMHC off-rates showed increased polyfunctional capacities (in terms of EC_{50} titration curves) when compared to the clones of fast TCR-pMHC off-rates (**Figure 2, B-D**). However, a strict correlation between off-rates and polyfunctionality was not always

found, and limited differences were mostly observed in the EBV-specific CD8 T cell responses. Taken together, the TCR-pMHC off-rate not only predicts single functional avidities of self/tumor- and virus-specific CD8 T cells, but also their capacity to co-develop multiple effector functions.

TCR-pMHC off-rate closely follows co-stimulatory/-inhibitory receptor expression in activated CD8 T cells

PD-1 surface expression on CD8 T cells has been reported to positively correlate with TCR-pMHC binding avidity (30) or functional avidity (31). Here, we explored the relationship between NTAmer-derived off-rates and the expression of various co-stimulatory (CD28 and CD137) and co-inhibitory (LAG-3, PD-1, TIGIT and TIM-3) receptors (**Figure 3**). No consistent correlations were found when CD8 T cell clones were assessed in a resting state (data not shown). In contrast, following 24 hours of stimulation with self/tumor or viral peptides, we observed substantial correlations between TCR-pMHC off-rates and the extent of increased expression of both co-stimulatory and -inhibitory receptors (**Figure 3, A-F**). These data indicate a direct impact of TCR-pMHC binding avidities on the susceptibility of CD8 T cells to antigen-specific activation, and consequently on the up-modulation of both co-stimulatory and -inhibitory receptors upon stimulation.

We also investigated whether TCR-pMHC off-rates associated with CD5 expression, which is a measure of the strength for self-pMHC selecting ligands during thymocyte development (32). At baseline, most virus-specific CD8 T cell clones displayed high expression levels of CD5, irrespective of their TCR-pMHC off-rates (**Figure 3G**). These data are in line with previous reports proposing that T cells with greater TCR's sensitivity to self pMHC are most efficiently recruited in response to foreign antigens (33, 34). Positive correlations were only

found in the context of self/tumor-specific CD8 T cell clones, with slower off-rates associating to higher baseline levels of CD5 (**Figure 3G** and **Supplemental Figure 5**). This latter observation suggest that the expression levels of CD5 on self/tumor-specific T cells may also predict their capacity for increased homeostatic or antigen-specific response.

TCR-pMHC off-rate predicts the in vivo functional potency of self/tumor-specific CD8 T cells

To further substantiate the relevance of our in vitro observations, we evaluated the impact of TCR-pMHC off-rates on the ability of self/tumor-specific CD8 T cells to control tumor growth in vivo. We first adoptively transferred A2/Melan-A_{26-35}-specific CD8 T cell clones of slow versus fast TCR-pMHC off-rates into immunodeficient NSG mice bearing human melanoma Me275 tumors (**Figure 4A**). The transfer of fast off-rate T cell clones showed intermediate tumor growth control. In contrast, T cell clones of slow off-rates mediated a more significant delay in tumor growth when compared to the untreated (PBS) group (**Figure 4B**). Furthermore, a significantly prolonged survival was only observed for mice treated with A2/Melan-A_{26-35}-specific clones of slow TCR-pMHC off-rates (**Figure 4C**). To confirm those observations, we then performed similar experiments using the A2/NY-ESO-1 antigenic model, but this time, all mice received s.c. injections of human recombinant IL-2 to enhance the T cell anti-tumor efficacy (**Figure 4D**). In line with the observations made on Melan-A_{26-35}-specific T cells, NY-ESO-$1_{157-165}$-specific CD8 T cell clones of slow TCR-pMHC off-rates provided a significant delay in tumor growth in comparison to the clones with fast off-rates (**Figure 4E**). Finally, we monitored the peripheral persistence of NY-ESO-1-specific T cells at days 2 and 14 following adoptive transfer. Analysis of tail bleeds taken at day 2 revealed that there was a significantly improved engraftment of slow off-rate T cell

clones compared with fast off-rate T cell clones (**Figure 4F**). Yet, tumor-specific T cells did not persist beyond 14 days after T cell transfer (data not shown), in line with a previous report (35). In summary, these data provide further evidence that the TCR-pMHC off-rate represents an excellent biomarker to predict the immunotherapeutic potential of tumor-specific CD8 T cells, and could therefore be selectively used to enhance the efficacy of adoptive T cell therapy (27).

TCR-pMHC off-rates vary according to the antigenic specificity of CD8 T cells

Only limited information is available on the overall quality of TCR-pMHC binding avidity of self/tumor- versus non-self/pathogen-specific CD8 T cell repertoires (36, 37). To address this point, we performed a comprehensive analysis of TCR-pMHC off-rates on 414 effector-memory CD8 T cell clones specific for (i) the differentiation antigen A2/Melan-A_{26-35}, (ii) the cancer testis antigen A2/NY-ESO-$1_{157-165}$, (iii) the viral CMV/$pp65_{495-504}$ antigen and (iv) the viral EBV/$BMFL1_{259-267}$ antigen isolated from five melanoma patients and two healthy donors (**Figure 5, A and B; Supplemental Figure 6, A and B**). TCR-pMHC off-rate repertoires varied according to the T cell antigenic specificity. As such, A2/Melan-A_{26-35} -specific CD8 T cells displayed significantly faster TCR-pMHC off-rates than the A2/NY-ESO-$1_{157-165}$-specific ones. Moreover, both tumor-specific TCR repertoires exhibited significantly faster TCR-pMHC off-rates than repertoires specific for herpes virus antigens (A2/$pp65_{495-504}$ and A2/$BMFL1_{259-267}$). Due to the presence of highly frequent TCR clonotypes potentially biasing the NY-ESO-1- and CMV-specific and to a lesser extent the EBV- and Melan-A-specific CD8 T cell repertoires (38-40), we performed an extensive TCR-BV-CDR3 clonotyping of 353 effector-memory CD8 T cell clones **(Figure 5C; Supplemental Table 1**). We identified 143 individual clonotypes (specific for A2/MelanA-

and A2/NYESO1-tumor antigens, and A2/pp65- and A2/BMLF1-viral epitopes), representing about 40% of the clonotype diversity, and depending on the antigenic specificity (Melan-A_{26-35} > EBV/$BMFL1_{259-267}$ > NY-ESO-$1_{157-165}$ and CMV/$pp65_{495-504}$). The same TCR-pMHC off-rate hierarchy (virus-specific > self/tumor-specific CD8 T cells) was observed when considering all CD8 T cell clones (**Figure 5B**) or only the individual TCR clonotypes (**Figure 5C**). Finally, similar differences were obtained when the CD8 T cell clones were subdivided according to their ex vivo differentiation status (early-differentiated EM/$CD28^+$ or late-differentiated EM/EMRA/$CD28^-$; **Supplemental Figure 6C**).

The differences found between A2/Melan-A_{26-35}- and A2/NY-ESO-$1_{157-165}$-specific repertoires may result from the fact that the A2/Melan-A_{26-35}-specific clones were derived following peptide vaccination combined to CpG and IFA adjuvant (41), when compared to the NY-ESO-1 repertoire obtained from patients with naturally-occurring T cell responses. Thus, we investigated the quality of the natural A2/MelanA_{26-35}-specific CD8 T cell repertoires found in unvaccinated melanoma patients (n = 2), as well as in A2-positive and A2-negative individuals without melanoma (n = 4), known to express an unusually large peripheral repertoire of naïve ($CD45RA^+CCR7^+$) A2/MelanA_{26-35}-reactive CD8 T cells (42). Unvaccinated patients exhibited differentiated A2/Melan-A_{26-35}-specific T cell repertoires of significantly faster off-rates when compared to the ones derived from vaccinated melanoma patients (**Figure 5D**). Strikingly, similar rapid off-rates were observed for the $CD45RA^+CCR7^+$ naïve-specific T cell repertoires derived from unvaccinated patients as well as from A2-positive and A2-negative healthy individuals. These observations reveal the overall inferior quality of the TCR-pMHC binding repertoires specific for the self-A2/Melan-A_{26-35} epitope, when compared to the ones specific for the cancer testis A2/NY-ESO-1 or viral antigens. Yet, several clones of slower off-rates could still be detected, indicating the presence of rare self/Melan-A-specific T cells of high binding avidity within the endogenous

unvaccinated repertoire. Finally, our data show that higher avidity T cells can be selected following therapeutic vaccination, emphasizing the relevance of therapeutic vaccination approaches in enhancing the quality of a tumor-specific repertoire.

TCR-pMHC off-rate is a stable and robust biomarker independent of the activation state of the T cell

CD8 T cell functional avidity represents a biological readout that is potentially influenced by multiple factors, such as TCR-pMHC binding avidity, TCR and CD8 surface expression as well as various molecules regulating TCR signaling and T cell function (10). In that regard, the TCR-pMHC off-rate may provide a more reliable biophysical parameter than the widely used functional-related methods to assess T cell potency. To investigate this question, we first compared the variations obtained following separate experimental measurements (n = 4 to 9) of TCR-based dissociation rates, multimer staining intensity levels and EC_{50} killing avidity of twelve representative Melan-A-specific CD8 T cell clones. For each individual clone, the inter-experimental off-rate values nicely clustered together, in sharp contrast to the repeat multimer staining and functional avidity experiments showing large disparities (**Figure 6, A-C)**. Furthermore, the average dissociation rates of these clones strongly correlated with average EC_{50} killing avidity, but not with average multimer staining intensity (**Supplemental Figure 7A**). Finally, no correlation was found between functional avidity and multimer staining levels, in agreement with previous reports (reviewed in (26)). We next performed longitudinal measurements of TCR-pMHC off-rates and EC_{50} killing avidity on a representative panel of A2/Melan-A_{26-35}-specific CD8 T cell clones following non-specific in vitro stimulation with PHA and feeder cells (**Supplemental Figure 7, B and C**). We observed a remarkable stability of TCR-pMHC off-rate measurements upon stimulation, even

when tested at a 6-month interval on T cell clones that underwent several additional rounds of PHA/feeder expansion (**Figure 6D**). In contrast and as previously described (43), for a given T cell clone, the killing avidity greatly varied and augmented up to 10-fold, according to the time elapsed since the last stimulation (**Figure 6E**). These data indicate that the functional avidity reflects the in vitro activation status of CD8 T cells, in line with the up-regulation of cell-surface expression of TCRαβ, CD8αβ, and VLA-1 integrin and, conversely the down-regulation of VLA-4 integrin and several co-inhibitory receptors such as CD5, LAG-3 and TIGIT or the co-stimulatory receptor CD28 (**Figure 6F**). Importantly, the TCR-pMHC binding off-rate measurement is independent of TCRαβ levels, and stands out as a more stable and reliable biomarker than the usually performed assessments of multimer staining levels (i.e. mean fluorescence intensity) or EC_{50} functional avidity.

DISCUSSION

Several observations support the importance of considering both quantitative (i.e. magnitude of response) and qualitative (i.e. functional avidity, polyfunctionality) determinants of the T cell response, in order to predict in vivo efficacy (reviewed in (10)). However, ex vivo functional avidity or EC_{50} (using titrated functional assays) and polyfunctionality assessments still remain laborious and time consuming, and often not possible because relatively large cell numbers must be withdrawn from patients. Importantly, and as shown in the current study, EC_{50} values largely depend on the T cell's activation state, and are thus influenced by intra-experimental (i.e. over time experimental measurements following T cell stimulation) and inter-experimental (i.e. separate experimental measurements) variability/fluctuations (**Figure 6**). Moreover, functional avidity varies greatly depending on the functional readouts (e.g. cytotoxicity versus cytokine production), which mostly reflects modulation of the function-specific activation thresholds (cytotoxicity < cytokine production) (**Figure 1, Supplemental Fig. 4A**). Taken together, there is a strong need to identify a T cell-based biomarker that overcomes the major limitations associated to functional assays and provides a reliable, simple to use, amenable to standardization immune metric for immunotherapy of cancer or chronic microbial infections.

Here, using an extensive and representative panel of antigen-specific CD8 T cells generated in the context of natural or post-vaccination immune responses, we show that the TCR-ligand dissociation rate globally correlated to all aspects of CD8 T cell functions tested (i.e. cytotoxic activity, CD107a degranulation, cytokine production, proliferation and co-receptor modulation; **Figure 1 and 3**), including polyfunctionality (**Figure 2**) of both self/tumor- and virus-specific CD8 T cells. Nonetheless, virus-specific T cells displayed weaker, although statistically significant correlations, than tumor-specific T cells, which may in part be the consequence of their overall slower TCR off-rates. These data nicely fit with the model

proposing that enhanced TCR affinity or off-rate correlates with improved T cell responsiveness, but that this correlation is no longer linear above a certain TCR binding avidity threshold (reviewed in (26)). Specifically, using artificial affinity-enhanced TCRs, several reports (30, 44, 45) have shown that maximal T cell responsiveness occurs within an optimal window of TCR-pMHC binding interactions, usually lying in the upper physiological affinity range (K_D between 10 to 1 μM), and encompassing naturally occurring non-self/virus-specific TCR repertoires (36, 37). Moreover, the monomeric TCR-pMHC off-rate also predicted the relative tumor control activity in vivo (**Figure 4**). Importantly, as a biophysical readout, the TCR-pMHC off-rate represents a more stable and robust parameter of T cell potency, compared to the fluctuating biological metrics, such as T cell functional avidity or multimer-staining levels, which instead depend on the activation status of the cell (**Figure 6**). Our observations are in agreement with other studies showing that functional avidity is not a constant parameter in individual T cell clones, but gradually increases with time after in vitro restimulation (43, 46) or during the early course of acute viral infection in vivo (47). Enhanced antigen sensitivity is notably influenced by the differential expression of TCRαβ and accessory molecules (i.e. increased CD8αβ and VLA-1 versus reduced CD28, LAG-3 and TIGIT expression) (**Figure 6**). Altogether, the TCR-pMHC off-rate stands out as a major and stable determinant of CD8 T cell function, allowing to accurately monitor the quality of naturally occurring or vaccinated-induced self/tumor-specific T cell responses, but also to identify the most potent CD8 T cells for adoptive transfer therapy.

Up-to-date, a debate remains regarding which parameter(s) of the TCR-pMHC interactions (e.g. K_D, k_{off}, k_{on}) could better predict T cell activation and subsequent response potency. Several studies reported that the dissociation rate (k_{off}) was the most significant factor (27, 45), whereas others proposed that the dissociation constant K_D was the preeminent correlate of T cell responsiveness (44, 48). However, the association rate parameter, k_{on}, may also

contribute to the response potency (49, 50). In that regard, Aleksic et al. (51) and Govern et al. (52) proposed that these apparently contradictory observations might in fact reflect the impact of fast versus slow association rates on the TCR-pMHC binding duration. Indeed, at the cell interface, fast k_{on} rates would allow rapid rebinding of the same TCR-ligand complex after dissociation, resulting in enhanced effective dissociation half-lives. Molecular TCR-pMHC binding interactions are usually assessed by SPR measurements in solution (3D binding), which fail to take into account the k_{on}-associated rapid rebinding effect of the TCR to the same pMHC. The NTAmer-based approach deviates in that regard from SPR measurements. Using a panel of CD8 T cells engineered to express TCR variants of increasing affinities for pMHC, we previously observed that TCRs with fast k_{on} had prolonged NTAmer-based dissociation half-lives compared to those with slow k_{on} (28). Thus, NTAmers may somehow reflect additional membrane-associated kinetic aspects (i.e. impact of rebinding and CD8 coreceptor), which are typically integrated by the 2D surface-based kinetic analyses (reviewed in (53)). Despite its current limitations (T cell cloning requirement, no direct k_{on} readouts), the NTAmer technology allows for rapid and accurate real-time off-rate measurements of large panels of naturally-occurring antigen-specific CD8 T cells, that may display a broad range of TCR-pMHC affinities, including weak interactions ((28, 29), current manuscript). Finally, a tight correlation between TCR off-rates and T cell antigenic sensitivity was not always observed, and notably depended on the antigenic specificity of the cells, but also on the T cell functional readout (**Figure 1 and 3**). However, robust statistical evaluation did not identify consistent outlier clones (i.e. the same clone that behaved as an outlier in one functional assay was not an outlier in the other functional assays). Thus, the few outlier data that we observed might best be explained by the variability/fluctuations related to biological measures (**Figure 6**), yet we cannot entirely exclude an impact of the k_{on} parameter, possibly influencing T cell responsiveness (49, 50).

In depth k_{on} evaluation of such exceptions would be highly useful, however only feasible once novel technologies that can interrogate all TCR-pMHC binding parameters directly on living T cells will become available.

Extending on previous studies showing a positive correlation between PD-1 expression and TCR-pMHC avidity (30) or functional avidity (31), NTAmer-based off-rates nicely predicted the up-modulation of both co-stimulatory (CD28, 4-1BB) and co-inhibitory (PD-1, LAG-3, TIM-3, TIGIT) receptors upon antigen-specific stimulation (**Figure 3**). Thus, our results indicate that T cells of higher binding avidity are more susceptible to activation and subsequent upregulation of activating/inhibitory receptors than lower avidity ones. Expression of inhibitory receptors such as PD-1 is usually considered as a hallmark of T cell exhaustion in chronic infection and cancer, and consequently high avidity T cells may be more prone to functional impairment. However, Odorizzi et al. (54) recently found that genetic absence of PD-1 on CD8 T cells does not prevent exhaustion during chronic LCMV infection. Instead, PD-1 also plays a critical role in protecting T cells from overstimulation, excessive proliferation and terminal differentiation (54) and identifies highly reactive anti-tumor T lymphocytes (55). Moreover, T cell differentiation and activation are major drivers of inhibitory receptor expression (56). Together, the extent of co-receptor up-modulation observed following stimulation **(Figure 3**) likely reveals the overall antigen sensitivity of the T cells, which is mostly driven by TCR-pMHC binding avidity.

Another major finding is that the TCR-pMHC dissociation rate parameter allows the direct comparison across various antigen-specific T cell repertoires, in contrast to functional assays. The latter ones rely on the stability of the pMHC complexes, which is not the case for monomeric TCR-pMHC dissociation experiments. Indeed, the stability of peptide binding to MHC may highly vary between different antigens even when presented by the same HLA-A*0201 molecule. This may help explaining why direct comparisons of in vitro functional

avidities (i.e. EC_{50}) between tumor- and virus-specific T cell clones, or between Melan-A_{26-35} and NY-ESO-$1_{157-165}$ or CMV/$pp65_{495-504}$ and EBV/$BMFL1_{259-267}$ specificities show such divergent differences (**Figure 1, Supplemental Fig. 4B**). For instance, Melan-A- and EBV-specific T cell clones generally exhibit the lowest EC_{50} functional avidities, whereas NY-ESO-1- and CMV-specific T cell clones share the highest ones. In contrast, this is no longer an issue for the off-rate measurements, which rely by definition on the dissociation rate between the TCR and a given pMHC complex at the monomeric level. Consequently, we were able to directly compare large T cell clonotype repertoires (n > 300) across four different antigenic specificities and confirm strong binding differences between self/tumor and virus-specific CD8 T cells (**Figure 5**; (36, 37)). Specifically, virus-specific CD8 T cell repertoires were endowed with longer TCR-pMHC dissociation-rates than self/tumor-specific one. These data nicely support the concept that many tumor antigens are in fact self-antigens, and consequently mechanisms of central and peripheral tolerance shape the self/antigen-specific repertoires towards lower TCR avidities by removing high-avidity self-reactive T cells (23, 57).

Fluorochrome-conjugated pMHC reagents are widely used for the detection and analysis of antigen-specific CD8 T cells. Various reports have previously shown that certain functional antigen-specific CD8 T cells fail to bind tetrameric MHC ligands, which could represent up to several percent of the CD8 T cell subset (58-60). Moreover, this is of particular importance when staining tumor-specific CD8 T cells, known to express lower TCR-pMHC affinity/avidity repertoires than virus-specific cells (**Figure 5**; (36, 37)). We therefore used pMHC multimer and NTAmer molecules to detect tumor-specific CD8 T cells, which consistently displayed higher sensitivity than Streptamers or Pentamers (**Supplemental Fig. 1A**) or pMHC tetramer molecules (data not shown). However, we cannot entirely exclude that a sizeable fraction of antigen-specific T cells may not be stained by these higher

sensitivity tools and may therefore be ignored in our experimental setting.

The Melan-A/MART-1 $_{26-35}$ antigenic peptide is among the best-studied human tumor-associated antigens. We have previously documented that the frequency of naive A2/Melan-A_{26-35}-specific CD8 T cells is unusually high, because of the large numbers selected in the thymus (42). A recent study reported that medullary thymic epithelial cells express a truncated *Melan-A* transcript, which precludes clonal deletion (central tolerance) to this antigen due to the lack of the expression of the immunodominant 26-35 epitope (61). Another interesting explanation might lay in the impact of certain germ line TCR gene segments, notably the *TRAV12-2* gene dominant in the Melan-A antigen specific T cell repertoire, on contributing substantial binding affinity for the HLA-A2/Melan-A 26-35 complex (62). One additional plausible cause of the presence of this large Melan-A_{26-35}-reactive T cell repertoire is that it could be positively selected through the recognition of unknown Melan-A cross-reactive peptides expressed in the thymus (63, 64). Here, we found that naive Melan-A_{26-35}-reactive repertoires isolated from either healthy individuals or unvaccinated melanoma patients depicted an overall poor TCR binding avidity, when compared to the primed repertoires from vaccinated patients (**Figure 5**). Thus, our observation are compatible with central tolerance mechanisms, possibly involving other cross-reactive self-antigens, and restricting the Melan-A_{26-35}-reactive T cell repertoire to the lower avidity range. Yet, although rare, our large-scale study could identify few self/ Melan-A_{26-35}-specific naive CD8 T cells of higher binding avidities within healthy individual's and patient's repertoires, extending and refining prior studies performed using conventional pMHC class-I fluorescent multimers (65). Therefore, it is possible that therapeutic vaccination allows for the selection and expansion of a wide Melan-A-reactive TCR avidity repertoire, which includes highly-specific T cells sharing similar binding avidities than those present in the cancer testis A2/NY-ESO-1-specific repertoire.

Finally, our results highlight the importance of optimizing the choice of tumor antigens for the development of cancer-based immunotherapies. Notably, it remains to be determined whether T cell repertoires targeting tumor-derived neoantigens can display greater TCR-pMHC binding avidities than self/tumor-antigen ones, since neoantigen-specific T cells are more likely to escape thymic negative selection (66). It is tempting to speculate that potent neoantigen-specific CD8 T cells would display TCR off-rates of magnitude closer to the kinetics of viral-specific CD8 T cells shown in this study.

Large-scale ex vivo assessment of TCR-pMHC binding kinetics was until recently technically challenging, underestimating the overall impact and clinical relevance of this biophysical parameter in the context of antigen-specific CD8 T cell repertoires. Based on monomeric TCR-pMHC off-rate measurements (i.e. NTAmers), we here demonstrated that the k_{off} parameter represents a powerful biomarker to characterize in vitro and in vivo CD8 T cell potency within antigen-specific CD8 T cell responses. Yet, robust techniques allowing for the rapid identification and isolation of CD8 T cells of highest avidity and functions directly ex vivo from tissues or blood samples and at the single cell level are still required. In that regard, Nauerth and colleagues (67) proposed that small polyclonal virus-specific CD8 T cell populations could be analyzed directly ex vivo without the need of previous TCR cloning or T cell sorting. The recent implementation of an ex vivo platform allowing for the single cell serial determination of 2D TCR-pMHC affinity (based on micropipette adhesion frequency) and TCR-clonotyping is also highly promising (68). In conclusion, recent technological breakthroughs now enable the rapid development of TCR-pMHC binding kinetics-based simple assays as sensitive and reliable biomarkers of CD8 T cell activity and clinical efficacy.

METHODS

Patients, healthy donors and ethics statement

Peripheral blood samples were collected from HLA-A*0201-negative (HD1 & HD2), HLA-A*0201-positive (HD3 & HD4), HLA-A*0201- positive and CMV/EBV-chronically infected (BCL4 & BCL6) healthy donors (HD) (39) and from HLA-A*0201-positive stage III/IV metastatic melanoma patients included in immunotherapy studies (patient LAU50; NCT00112242, patient LAU155; NCT00002669, and patients LAU975, LAU1013, LAU618, LAU627 and LAU818; NCT00112229; www.clinicaltrials.gov) (38, 41, 69). Patients LAU618, LAU627 and LAU818 received 8 to 12 monthly low-dose vaccinations injected s.c. with 100 μg high-affinity Melan-$A_{26\text{-}35\ (A27L)}$ analog peptide mixed with 0.5 mg CpG 7909/PF-3512676 (Pfizer and Coley Pharmaceutical Group) and emulsified in IFA (Montanide ISA-51, Seppic). Ficoll-Hypaque (Pharmacia, Uppsala, Sweden) centrifuged peripheral blood mononuclear cells (PBMCs) were cryopreserved in 10% DMSO and stored in liquid nitrogen until further use.

Generation of antigen-specific CD8 T cell clones

Thawed PBMCs were positively enriched using anti-CD8-coated magnetic microbeads (Miltenyi Biotec), stained in PBS, 0.2% BSA and 5 mM EDTA with PE-labeled HLA-A*0201 multimers (loaded with analog Melan-$A_{26–35(A27L)}$, NY-ESO-$1_{157\text{-}165(C165A)}$, and EBV/BMFL$1_{259\text{-}267(C260A)}$, or native CMV/pp$65_{495\text{-}504}$ peptide) (TCMetrix Sàrl) at 4°C for 45 min, followed by cell surface markers (APC anti-CD28, FITC anti-CD45RA (BD Pharmingen), PE-Cy7 anti-CCR7 (BioLegend), APC-A750 anti-CD8 (Beckman Coulter), **Supplemental Table 2**) at 4°C for 30 min. Cells were then sorted into defined differentiated subpopulations (naïve, $CD45RA^+CCR7^+CD28^+$; effector-memory (EM) $CD45RA^-CCR7^-CD28^{+/-}$ or EMRA, $CD45RA^+CCR7^-CD28^-$) of antigen-specific CD8 T cells on a FACSAria

(BD Biosciences) or Astrios (Beckman Coulter) flow cytometer. Sorted cells were cloned by limiting dilution in Terasaki plates and expanded in RPMI 1640 medium supplemented with 8% human serum, 150 U/ml human rIL-2 (gift of GlaxoSmithKline), 1 μg/ml PHA (Sodiag) and $1x10^6$/ml 30-Gy irradiated allogeneic PBMCs. The antigenic specificity of CD8 T cell clones was controlled by HLA-A*0201/peptide multimer stainings (TCMetrix Sàrl). Extensive TCR-BV-CDR3 clonotyping was performed on the T cells from patients LAU618, LAU155 and LAU50 and from healthy donors BCL4 & BCL6, as previously described (39), allowing selecting representative sets of dominant (with frequency >5%) and non-dominant TCR-BV-CDR3 clonotypes. Clonotype diversity varied from 43% to 80%, depending on the antigenic specificity (Melan-$A_{26–35}$ > EBV/BMFL1$_{259-267}$ > NY-ESO-1$_{157-165}$ and CMV/pp65$_{495-504}$) and is indicated throughout the manuscript.

NTAmer staining and dissociation kinetic measurements

The pMHC multimer and NTAmer molecules used in this study carry 8 to 12 pMHC monomers per conjugate, similarly to Dextramer molecules. Importantly, multimers and NTAmers provided a superior ex vivo detection of A2/MelanA-specific CD8 T cells from PBMCs of two melanoma patients, when compared to Pentamers (5 pMHC monomers) or Streptamers (5-7 pMHC monomers) (**Supplemental Figure 1A**). NTAmers are dually labeled pMHC multimers built on NTA-Ni2+-His-tag interactions (70) and were used for dissociation kinetic measurements as described previously (28, 29). Briefly, individual antigen-specific CD8 T cell clones were stained for 45 min at 4°C in PBS, 0.2% BSA and 5 mM EDTA with antigen-specific NTAmers, in which the HLA-A*0201 molecules were loaded with the native Melan-$A_{26–35}$, NY-ESO-1$_{157-165}$, EBV/BMFL1$_{259-267}$, or CMV/pp65$_{495-504}$ peptide. Of note, Melan-A- and NY-ESO-1-specific T cells isolated from melanoma patients as well as EBV-specific T cells from healthy donor BCL4 were initially sorted with

the analog-peptide multimers. Yet, all Melan-A-, NY-ESO1- and EBV-derived T cell clones presented a high degree of cross-reactivity, since native-peptide NTAmers showed a comparable capacity to stably label each generated specific clone and thus should not have introduced a significant bias in the analysis. NTAmer staining was assessed at 4°C on a SORP-LSR II flow cytometer (BD Biosciences). Following 1 min of baseline acquisition, imidazole (100 mM) was added and Cy5 fluorescence measured during the following 10 min. Data were analyzed using the kinetic module of the FlowJo software (v.9.7.6, Tree Star) and modeled (one phase exponential decay) using the Prism software (v.6, GraphPad).

Chromium release cytolytic assay

Chromium release cytolytic assays were performed as previously described (13). Briefly, ^{51}Cr-labeled HLA-A*0201-positive TAP-deficient T2 cells were pulsed with serial dilutions of native Melan-$A_{26–35}$, NY-ESO-$1_{157-165,}$ EBV/BMFL$1_{259-267,}$ or CMV/pp$65_{495-504}$ peptides, and incubated with antigen-specific CD8 T cell clones at an E:T ratio of 10:1 for 4h. NY-ESO-$1_{157-165}$ and EBV BMFL$1_{259-267}$ peptides were pre-incubated for 1h at room temperature with 2 mM of disulfide-reducing agent Tris [2-carboxyethyl] phosphine (TCEP, Pierce Biotechnology). Percentages of specific lysis were calculated as 100 x (experimental - spontaneous release)/(total - spontaneous release). EC_{50} and B_{max} values were derived by dose-response curve analysis (log(agonist) versus response) using the Prism software (v.6, GraphPad). Non-killer clones were defined as displaying a maximal lysis <25% and/or for which an EC_{50} value could not be accurately determined. These non-killer clones were excluded from the statistical analyses.

CD107a degranulation & intracellular cytokine staining

HLA-A*0201-positive TAP-deficient T2 cells were pulsed 1h at 37°C with serial dilutions of the native Melan-$A_{26–35}$, NY-ESO-$1_{157-165,}$ EBV/BMFL$1_{259-267,}$ or CMV/pp$65_{495-504}$ peptides,

washed and incubated with antigen-specific CD8 T cell clones at an E:T ratio of 1:2 for 6h in the presence of FITC anti-CD107a (BD Pharmingen; **Supplemental Table 2**) and Brefeldin A (10μg/ml, Sigma). NY-ESO-$1_{157\text{-}165}$ and EBV BMFL$1_{259\text{-}267}$ peptide were pre-incubated for 1h at room temperature with the disulfide-reducing agent TCEP (2 mM; Pierce Biotechnology). Cells were then stained in PBS, 0.2% BSA, 5 mM EDTA and 0.2% NaN_3 with Pacific-Blue anti-CD8α (Beckman Coulter) at 4°C for 30 min, fixed in PBS 1% formaldehyde, 2% glucose and 5 mM NaN_3 for 20 min at RT, and finally stained in PBS, 0.2% BSA, 5 mM EDTA, 0.2% NaN_3 and 0.1% Saponin (Sigma) with PerCPCy5.5 anti-IL-2, APC anti-IL-13, PE-Cy7 anti-IFNγ, A700 anti-TNFα (BD Pharmingen; **Supplemental Table 2**) and PE anti-IL-4 (Biolegend) for 30 min at 4°C before acquisition on a Gallios (Beckman Coulter) flow cytometer. Percentages of CD107a/cytokine-positive T cells were analyzed using the FlowJo software (v.10.0.7, Tree Star). EC_{50} and B_{max} values were derived by dose-response curve analysis (log(agonist) versus response) using the Prism software (v.6, GraphPad). Non-cytokine clones were defined as displaying a maximal response <25% and for which an EC_{50} value could not be determined accurately. These non-cytokine clones were not included in the statistical analyses. CD107a, IL-2, IFNγ and TNFα□CO-expression were analyzed using the SPICE software (v.5.35, National Institute of Allergy & Infectious Diseases).

Proliferation assay

30-Gy irradiated HLA-A*0201-positive PBMCs were pulsed 1h at 37°C with native Melan-$A_{26–35}$ (10 μM), NY-ESO-$1_{157\text{-}165}$ (1 μM), EBV/BMFL$1_{259\text{-}267}$ (1 μM), or CMV/pp$65_{495\text{-}504}$ peptides (0.01 μM), washed and incubated with CellTraceViolet-stained antigen-specific CD8 T cell clones (ThermoFischer) at an E:T ratio of 1:2 in RPMI 1640 medium supplemented with 8% human serum and 50 U/ml human rIL-2 (gift of GlaxoSmithKline).

NY-ESO-$1_{157\text{-}165}$ and EBV/BMFL$1_{259\text{-}267}$ peptides were pre-incubated for 1h at room temperature with the disulfide-reducing agent TCEP (2 mM, Pierce Biotechnology). After 7 days, antigen-specific CD8 T cell clones were acquired on a Gallios (Beckman Coulter) flow cytometer. Percentages of divided cells were analyzed using the proliferation module of the FlowJo software (v.9.7.6, Tree Star).

Surface marker expression/modulation assay

For co-receptor modulation assays, antigen-specific CD8 T cell clones were incubated for 24h in the absence or presence of HLA-A*0201 unlabeled tetramers loaded with native Melan-$A_{26–35}$ (1 µg/ml), NY-ESO-$1_{157\text{-}165}$ (1 µg/ml), EBV BMFL$1_{259\text{-}267}$ (0.1 µg/ml), or CMV $pp65_{495\text{-}504}$ (0.01 µg/ml) peptides. Cells were then stained in PBS, 0.2% BSA, 5 mM EDTA and 0.2% NaAzide with (i) A488 anti-PD1 (Serotec), PE-Cy7 anti-CD5 (BD Pharmingen), APC anti-TIGIT (eBioscience) and BrV421 anti-CD28 (Biolegend), or with (ii) FITC anti-LAG-3 (Enzo), PE anti-TIM-3 (R&D Systems) and APC anti-CD137 (BD Pharmingen) at 4°C for 30 min and acquired on a Gallios (Beckman Coulter) flow cytometer. Markers expression (gMFI) was analyzed using the FlowJo software (v.10.0.7, Tree Star) and their modulation was calculated as (gMFI of stimulated cells) / (gMFI of un-stimulated cells).

For over time expression assays, tumor-specific CD8 T cell clones were stimulated and expanded upon PHA and irradiated feeder cells, and stained overtime (at day 10, 15 and 20) in PBS, 0.2% BSA, 5 mM EDTA and 0.2% NaAzide with FITC anti-CD8β, PE-Cy7 anti-CD8α, PE anti-pan-TCRαβ (Beckman Coulter), PE anti-VLA-1, PE-Cy7 anti-CD5, APC anti-VLA-4, APC anti-CD137, BrV421 anti-PD1 (BD Pharmingen), APC anti-TIGIT (eBioscience), BrV421 anti-CD28 (Biolegend) or FITC anti-LAG-3 (Enzo) at 4°C for 30 min, and acquired, using identical settings, on a Gallios (Beckman Coulter) flow cytometer.

Supplemental Table 2 contains a detailed list and information of all antibodies used in this study.

Adoptive T cell transfer in immunodeficient mice

NSG (NOD.Cg-Prkdc^{scid} Il2rg^{tm1Wjl}/SzJ) mice (Jackson, stock number 005557) were bred in the conventional animal facility of the University of Lausanne under SPF status. Six to nine weeks old female mice were anesthetized with isofluran and subcutaneously injected with $1x10^6$ A2/Melan-$A_{26–35}$- and A2/NY-ESO-$1_{157-165}$-positive human melanoma Me275 tumor cells (grown in DMEM medium supplemented with 10% FCS, and previously passed in NSG mice for A2/NY-ESO-$1_{157-165}$-specific experiments). Once the tumors became palpable (around D14 to 20), $1x10^6$ human tumor-specific CD8 T cell clones were injected intravenously in the tail vein. For A2/NY-ESO-$1_{157-165}$-specific experiments, $1x10^6$ T cell clones were administrated twice at D14 and D21, followed by 3 daily subcutaneously injections of human rIL-2 ($3x10^4$ U; gift of GlaxoSmithKline), starting at the day of T cell transfer. Tumor volumes were measured by caliper twice a week and calculated as follow: volume = length x width x width/2. Mice were sacrificed by CO_2 inhalation before the tumor volume exceeded 1000 mm^3 or when necrotic skin lesions were observed at the tumor site. In separate experiments, we collected blood from tail veins at D2 and D14 after infusion of $4x10^6$ A2/NY-ESO-$1_{157-165}$-specific T cell clones and analyzed the frequency of persisting human CD8 T cells by flow cytometry. This study was approved by the Veterinary Authority of the Canton de Vaud (Permit n°VD1850.5) and performed in accordance with Swiss ethical guidelines.

Statistical analysis

Data were analyzed using the Prism software (v.7, GraphPad) by non-parametric Spearman correlation, non-linear regression (95% confidence intervals and 10% ROUT coefficient Q

(71)), extra sum-of-squares F, Kruskal-Wallis, Mann-Whitney, Friedman, Wilcoxon-paired, two-way ANOVA and log-rank tests. The associated *p* values (two-tailed and $\alpha = 0.05$ when applicable), as well as numbers of experiments and sample sizes are indicated throughout the manuscript.

Study approvals

Study protocols were designed, approved and conducted according to the relevant regulatory standards from (i) the ethical commission of the University of Lausanne (Lausanne, Switzerland), (ii) the Protocol Review Committee of the Ludwig Institute for Cancer Research (New-York) and (iii) Swissmedic (Bern, Switzerland). Healthy donors and patient recruitment, study procedures and blood withdrawal were done upon written informed consent.

AUTHOR CONTRIBUTIONS

Conception and design: MA, JS, MH and NR. Acquisition of data (provided animals, acquired and managed patients, provided facilities, etc.): MA, BC, LCI, MND, JS, GM, PR, DES and MH. Analysis and interpretation of data: MA, MH and NR. Writing and/or revision of the manuscript: MA, PR, DES, MH and NR. Study supervision: NR.

ACKNOWLEDGMENTS

The authors thank the patients and the healthy donors for their dedicated collaboration to this study. They gratefully acknowledge N. Montandon and P. Werffeli for excellent technical and secretarial help, and P. Baumgaertner, A. Donda, P. Gannon and K. Ioannidou for collaboration and advice. This study was sponsored and supported by the ISREC Foundation (Switzerland), the MEDIC Foundation (Switzerland), the Promedica Foundation (Switzerland), the Swiss National Science Foundation (310030-1159417, 31003A-156469 and Sinergia CRSII3-160708), and the Wilhelm Sander-Foundation (Germany).

REFERENCES

1. Speiser DE, Kyburz D, Stubi U, Hengartner H, and Zinkernagel RM. Discrepancy between in vitro measurable and in vivo virus neutralizing cytotoxic T cell reactivities. Low T cell receptor specificity and avidity sufficient for in vitro proliferation or cytotoxicity to peptide-coated target cells but not for in vivo protection. *J Immunol.* 1992;149(3):972-980.

2. Alexander-Miller MA, Leggatt GR, and Berzofsky JA. Selective expansion of high- or low-avidity cytotoxic T lymphocytes and efficacy for adoptive immunotherapy. *Proceedings of the National Academy of Sciences of the United States of America.* 1996;93(9):4102-4107.

3. Gallimore A, Dumrese T, Hengartner H, Zinkernagel RM, and Rammensee HG. Protective immunity does not correlate with the hierarchy of virus-specific cytotoxic T cell responses to naturally processed peptides. *J Exp Med.* 1998;187(10):1647-1657.

4. Zeh HJ, 3rd, Perry-Lalley D, Dudley ME, Rosenberg SA, and Yang JC. High avidity CTLs for two self-antigens demonstrate superior in vitro and in vivo antitumor efficacy. *J Immunol.* 1999;162(2):989-994.

5. Bullock TN, Mullins DW, Colella TA, and Engelhard VH. Manipulation of avidity to improve effectiveness of adoptively transferred CD8(+) T cells for melanoma immunotherapy in human MHC class I-transgenic mice. *J Immunol.* 2001;167(10):5824-5831.

6. Almeida JR, Price DA, Papagno L, Arkoub ZA, Sauce D, Bornstein E, et al. Superior control of HIV-1 replication by CD8+ T cells is reflected by their avidity, polyfunctionality, and clonal turnover. *J Exp Med.* 2007;204(10):2473-2485.

7. Berger CT, Frahm N, Price DA, Mothe B, Ghebremichael M, Hartman KL, et al. High-functional-avidity cytotoxic T lymphocyte responses to HLA-B-restricted Gag-derived epitopes associated with relative HIV control. *J Virol.* 2011;85(18):9334-9345.

8. Yerly D, Heckerman D, Allen TM, Chisholm JV, 3rd, Faircloth K, Linde CH, et al. Increased cytotoxic T-lymphocyte epitope variant cross-recognition and functional avidity are associated with hepatitis C virus clearance. *J Virol.* 2008;82(6):3147-3153.

9. Neveu B, Debeaupuis E, Echasserieau K, le Moullac-Vaidye B, Gassin M, Jegou L, et al. Selection of high-avidity CD8 T cells correlates with control of hepatitis C virus infection. *Hepatology.* 2008;48(3):713-722.

10. Vigano S, Utzschneider DT, Perreau M, Pantaleo G, Zehn D, and Harari A. Functional avidity: a measure to predict the efficacy of effector T cells? *Clin Dev Immunol.* 2012;2012(153863.

11. Dudley ME, Nishimura MI, Holt AK, and Rosenberg SA. Antitumor immunization with a minimal peptide epitope (G9-209-2M) leads to a functionally heterogeneous CTL response. *J Immunother.* 1999;22(4):288-298.

12. Dutoit V, Rubio-Godoy V, Dietrich PY, Quiqueres AL, Schnuriger V, Rimoldi D, et al. Heterogeneous T-cell response to MAGE-A10(254-262): high avidity-specific cytolytic T lymphocytes show superior antitumor activity. *Cancer Res.* 2001;61(15):5850-5856.

13. Speiser DE, Baumgaertner P, Barbey C, Rubio-Godoy V, Moulin A, Corthesy P, et al. A novel approach to characterize clonality and differentiation of human melanoma-specific T cell responses: spontaneous priming and efficient boosting by vaccination. *J Immunol.* 2006;177(2):1338-1348.

14. Betts MR, Nason MC, West SM, De Rosa SC, Migueles SA, Abraham J, et al. HIV nonprogressors preferentially maintain highly functional HIV-specific CD8+ T cells. *Blood.* 2006;107(12):4781-4789.

15. Harari A, Petitpierre S, Vallelian F, and Pantaleo G. Skewed representation of functionally distinct populations of virus-specific CD4 T cells in HIV-1-infected subjects with progressive disease: changes after antiretroviral therapy. *Blood.* 2004;103(3):966-972.

16. Ciuffreda D, Comte D, Cavassini M, Giostra E, Buhler L, Perruchoud M, et al. Polyfunctional HCV-specific T-cell responses are associated with effective control of HCV replication. *Eur J Immunol.* 2008;38(10):2665-2677.

17. Wilde S, Sommermeyer D, Leisegang M, Frankenberger B, Mosetter B, Uckert W, and Schendel DJ. Human antitumor CD8+ T cells producing Th1 polycytokines show superior antigen sensitivity and tumor recognition. *J Immunol.* 2012;189(2):598-605.

18. Almeida JR, Sauce D, Price DA, Papagno L, Shin SY, Moris A, et al. Antigen sensitivity is a major determinant of CD8+ T-cell polyfunctionality and HIV-suppressive activity. *Blood.* 2009;113(25):6351-6360.

19. Clay TM, Hobeika AC, Mosca PJ, Lyerly HK, and Morse MA. Assays for monitoring cellular immune responses to active immunotherapy of cancer. *Clin Cancer Res.* 2001;7(5):1127-1135.

20. Keilholz U, Martus P, and Scheibenbogen C. Immune monitoring of T-cell responses in cancer vaccine development. *Clin Cancer Res.* 2006;12(7 Pt 2):2346s-2352s.

21. Moran AE, and Hogquist KA. T-cell receptor affinity in thymic development. *Immunology.* 2012;135(4):261-267.

22. Ozga AJ, Moalli F, Abe J, Swoger J, Sharpe J, Zehn D, Kreutzfeldt M, Merkler D, Ripoll J, and Stein JV. pMHC affinity controls duration of CD8+ T cell-DC interactions and imprints timing of effector differentiation versus expansion. *J Exp Med.* 2016;213(12):2811-2829.

23. Zehn D, and Bevan MJ. T cells with low avidity for a tissue-restricted antigen routinely evade central and peripheral tolerance and cause autoimmunity. *Immunity.* 2006;25(2):261-270.

24. Hebeisen M, Oberle SG, Presotto D, Speiser DE, Zehn D, and Rufer N. Molecular insights for optimizing T cell receptor specificity against cancer. *Front Immunol.* 2013;4(154.

25. Stone JD, Chervin AS, and Kranz DM. T-cell receptor binding affinities and kinetics: impact on T-cell activity and specificity. *Immunology.* 2009;126(2):165-176.

26. Hebeisen M, Allard M, Gannon PO, Schmidt J, Speiser DE, and Rufer N. Identifying Individual T Cell Receptors of Optimal Avidity for Tumor Antigens. *Front Immunol.* 2015;6(582.

27. Nauerth M, Weissbrich B, Knall R, Franz T, Dossinger G, Bet J, et al. TCR-ligand koff rate correlates with the protective capacity of antigen-specific CD8+ T cells for adoptive transfer. *Sci Transl Med.* 2013;5(192):192ra187.

28. Hebeisen M, Schmidt J, Guillaume P, Baumgaertner P, Speiser DE, Luescher I, and Rufer N. Identification of Rare High-Avidity, Tumor-Reactive CD8+ T Cells by Monomeric TCR-Ligand Off-Rates Measurements on Living Cells. *Cancer Res.* 2015;75(10):1983-1991.

29. Gannon PO, Wieckowski S, Baumgaertner P, Hebeisen M, Allard M, Speiser DE, and Rufer N. Quantitative TCR:pMHC Dissociation Rate Assessment by NTAmers Reveals Antimelanoma T Cell Repertoires Enriched for High Functional Competence. *J Immunol.* 2015;195(1):356-366.

30. Hebeisen M, Baitsch L, Presotto D, Baumgaertner P, Romero P, Michielin O, Speiser DE, and Rufer N. SHP-1 phosphatase activity counteracts increased T cell receptor affinity. *J Clin Invest.* 2013;123(3):1044-1056.

31. Simon S, Vignard V, Florenceau L, Dreno B, Khammari A, Lang F, and Labarriere N. PD-1 expression conditions T cell avidity within an antigen-specific repertoire. *Oncoimmunology.* 2016;5(1):e1104448.

32. Azzam HS, Grinberg A, Lui K, Shen H, Shores EW, and Love PE. CD5 expression is developmentally regulated by T cell receptor (TCR) signals and TCR avidity. *J Exp Med.* 1998;188(12):2301-2311.

33. Mandl JN, Monteiro JP, Vrisekoop N, and Germain RN. T cell-positive selection uses self-ligand binding strength to optimize repertoire recognition of foreign antigens. *Immunity.* 2013;38(2):263-274.

34. Fulton RB, Hamilton SE, Xing Y, Best JA, Goldrath AW, Hogquist KA, and Jameson SC. The TCR's sensitivity to self peptide-MHC dictates the ability of naive CD8(+) T cells to respond to foreign antigens. *Nat Immunol.* 2015;16(1):107-117.

35. Straetemans T, Coccoris M, Berrevoets C, Treffers-Westerlaken E, Scholten CE, Schipper D, Ten Hagen TL, and Debets R. T-cell receptor gene therapy in human melanoma-bearing immune-deficient mice: human but not mouse T cells recapitulate outcome of clinical studies. *Hum Gene Ther.* 2012;23(2):187-201.

36. Aleksic M, Liddy N, Molloy PE, Pumphrey N, Vuidepot A, Chang KM, and Jakobsen BK. Different affinity windows for virus and cancer-specific T-cell receptors: implications for therapeutic strategies. *Eur J Immunol.* 2012;42(12):3174-3179.

37. Cole DK, Pumphrey NJ, Boulter JM, Sami M, Bell JI, Gostick E, Price DA, Gao GF, Sewell AK, and Jakobsen BK. Human TCR-binding affinity is governed by MHC class restriction. *J Immunol.* 2007;178(9):5727-5734.

38. Derre L, Bruyninx M, Baumgaertner P, Ferber M, Schmid D, Leimgruber A, et al. Distinct sets of alphabeta TCRs confer similar recognition of tumor antigen NY-ESO-1157-165 by interacting with its central Met/Trp residues. *Proceedings of the National Academy of Sciences of the United States of America.* 2008;105(39):15010-15015.

39. Iancu EM, Corthesy P, Baumgaertner P, Devevre E, Voelter V, Romero P, Speiser DE, and Rufer N. Clonotype selection and composition of human CD8 T cells specific for persistent herpes viruses varies with differentiation but is stable over time. *J Immunol.* 2009;183(1):319-331.

40. Speiser DE, Wieckowski S, Gupta B, Iancu EM, Baumgaertner P, Baitsch L, Michielin O, Romero P, and Rufer N. Single cell analysis reveals similar functional competence of dominant and nondominant CD8 T-cell clonotypes. *Proceedings of the National Academy of Sciences of the United States of America.* 2011;108(37):15318-15323.

41. Speiser DE, Baumgaertner P, Voelter V, Devevre E, Barbey C, Rufer N, and Romero P. Unmodified self antigen triggers human CD8 T cells with stronger tumor reactivity than altered antigen. *Proceedings of the National Academy of Sciences of the United States of America.* 2008;105(10):3849-3854.

42. Romero P, Speiser DE, and Rufer N. Deciphering the unusual HLA-A2/Melan-A/MART-1-specific TCR repertoire in humans. *Eur J Immunol.* 2014;44(9):2567-2570.

43. Hesse MD, Karulin AY, Boehm BO, Lehmann PV, and Tary-Lehmann M. A T cell clone's avidity is a function of its activation state. *J Immunol.* 2001;167(3):1353-1361.

44. Tan MP, Gerry AB, Brewer JE, Melchiori L, Bridgeman JS, Bennett AD, et al. T cell receptor binding affinity governs the functional profile of cancer-specific CD8+ T cells. *Clin Exp Immunol.* 2015;180(2):255-270.

45. Kalergis AM, Boucheron N, Doucey MA, Palmieri E, Goyarts EC, Vegh Z, Luescher IF, and Nathenson SG. Efficient T cell activation requires an optimal dwell-time of interaction between the TCR and the pMHC complex. *Nat Immunol.* 2001;2(3):229-234.

46. Falcioni F, Shah H, Vidovic D, Morimoto C, Belunis C, Bolin D, and Nagy ZA. Influence of CD26 and integrins on the antigen sensitivity of human memory T cells. *Hum Immunol.* 1996;50(2):79-90.

47. Slifka MK, and Whitton JL. Functional avidity maturation of CD8(+) T cells without selection of higher affinity TCR. *Nat Immunol.* 2001;2(8):711-717.

48. Tian S, Maile R, Collins EJ, and Frelinger JA. CD8+ T cell activation is governed by TCR-peptide/MHC affinity, not dissociation rate. *J Immunol.* 2007;179(5):2952-2960.

49. Huang J, Zarnitsyna VI, Liu B, Edwards LJ, Jiang N, Evavold BD, and Zhu C. The kinetics of two-dimensional TCR and pMHC interactions determine T-cell responsiveness. *Nature.* 2010;464(7290):932-936.

50. Huppa JB, Axmann M, Mortelmaier MA, Lillemeier BF, Newell EW, Brameshuber M, Klein LO, Schutz GJ, and Davis MM. TCR-peptide-MHC interactions in situ show accelerated kinetics and increased affinity. *Nature.* 2010;463(7283):963-967.

51. Aleksic M, Dushek O, Zhang H, Shenderov E, Chen JL, Cerundolo V, Coombs D, and van der Merwe PA. Dependence of T cell antigen recognition on T cell receptor-peptide MHC confinement time. *Immunity.* 2010;32(2):163-174.

52. Govern CC, Paczosa MK, Chakraborty AK, and Huseby ES. Fast on-rates allow short dwell time ligands to activate T cells. *Proceedings of the National Academy of Sciences of the United States of America.* 2010;107(19):8724-8729.

53. Zhu C, Jiang N, Huang J, Zarnitsyna VI, and Evavold BD. Insights from in situ analysis of TCR-pMHC recognition: response of an interaction network. *Immunol Rev.* 2013;251(1):49-64.

54. Odorizzi PM, Pauken KE, Paley MA, Sharpe A, and Wherry EJ. Genetic absence of PD-1 promotes accumulation of terminally differentiated exhausted CD8+ T cells. *J Exp Med.* 2015;212(7):1125-1137.

55. Gros A, Robbins PF, Yao X, Li YF, Turcotte S, Tran E, et al. PD-1 identifies the patient-specific CD8(+) tumor-reactive repertoire infiltrating human tumors. *J Clin Invest.* 2014;124(5):2246-2259.

56. Legat A, Speiser DE, Pircher H, Zehn D, and Fuertes Marraco SA. Inhibitory Receptor Expression Depends More Dominantly on Differentiation and Activation than "Exhaustion" of Human CD8 T Cells. *Front Immunol.* 2013;4(455.

57. Bouneaud C, Kourilsky P, and Bousso P. Impact of negative selection on the T cell repertoire reactive to a self-peptide: a large fraction of T cell clones escapes clonal deletion. *Immunity.* 2000;13(6):829-840.

58. Tungatt K, Bianchi V, Crowther MD, Powell WE, Schauenburg AJ, Trimby A, et al. Antibody stabilization of peptide-MHC multimers reveals functional T cells bearing extremely low-affinity TCRs. *J Immunol.* 2015;194(1):463-474.

59. Khan N, Cobbold M, Cummerson J, and Moss PA. Persistent viral infection in humans can drive high frequency low-affinity T-cell expansions. *Immunology.* 2010;131(4):537-548.

60. Huang J, Zeng X, Sigal N, Lund PJ, Su LF, Huang H, Chien YH, and Davis MM. Detection, phenotyping, and quantification of antigen-specific T cells using a peptide-MHC dodecamer. *Proceedings of the National Academy of Sciences of the United States of America.* 2016;113(13):E1890-1897.

61. Pinto S, Sommermeyer D, Michel C, Wilde S, Schendel D, Uckert W, Blankenstein T, and Kyewski B. Misinitiation of intrathymic MART-1 transcription and biased TCR usage explain the high frequency of MART-1-specific T cells. *Eur J Immunol.* 2014;44(9):2811-2821.

62. Cole DK, Yuan F, Rizkallah PJ, Miles JJ, Gostick E, Price DA, Gao GF, Jakobsen BK, and Sewell AK. Germ line-governed recognition of a cancer epitope by an immunodominant human T-cell receptor. *J Biol Chem.* 2009;284(40):27281-27289.

63. Loftus DJ, Castelli C, Clay TM, Squarcina P, Marincola FM, Nishimura MI, Parmiani G, Appella E, and Rivoltini L. Identification of epitope mimics recognized by CTL reactive to the melanoma/melanocyte-derived peptide MART-1(27-35). *J Exp Med.* 1996;184(2):647-657.

64. Dutoit V, Rubio-Godoy V, Pittet MJ, Zippelius A, Dietrich PY, Legal FA, et al. Degeneracy of antigen recognition as the molecular basis for the high frequency of naive A2/Melan-a peptide multimer(+) CD8(+) T cells in humans. *J Exp Med.* 2002;196(2):207-216.

65. Pittet MJ, Rubio-Godoy V, Bioley G, Guillaume P, Batard P, Speiser D, Luescher I, Cerottini JC, Romero P, and Zippelius A. Alpha 3 domain mutants of peptide/MHC class I multimers allow the selective isolation of high avidity tumor-reactive CD8 T cells. *J Immunol.* 2003;171(4):1844-1849.

66. Schumacher TN, and Schreiber RD. Neoantigens in cancer immunotherapy. *Science.* 2015;348(6230):69-74.

67. Nauerth M, Stemberger C, Mohr F, Weissbrich B, Schiemann M, Germeroth L, and Busch DH. Flow cytometry-based TCR-ligand Koff -rate assay for fast avidity screening of even very small antigen-specific T cell populations ex vivo. *Cytometry A.* 2016;89(9):816-825.

68. Zhang SQ, Parker P, Ma KY, He C, Shi Q, Cui Z, et al. Direct measurement of T cell receptor affinity and sequence from naive antiviral T cells. *Sci Transl Med.* 2016;8(341):341ra377.

69. Speiser DE, Lienard D, Rufer N, Rubio-Godoy V, Rimoldi D, Lejeune F, Krieg AM, Cerottini JC, and Romero P. Rapid and strong human CD8+ T cell responses to vaccination with peptide, IFA, and CpG oligodeoxynucleotide 7909. *J Clin Invest.* 2005;115(3):739-746.

70. Schmidt J, Guillaume P, Irving M, Baumgaertner P, Speiser D, and Luescher IF. Reversible major histocompatibility complex I-peptide multimers containing Ni(2+)-nitrilotriacetic acid peptides and histidine tags improve analysis and sorting of CD8(+) T cells. *J Biol Chem.* 2011;286(48):41723-41735.

71. Motulsky HJ, and Brown RE. Detecting outliers when fitting data with nonlinear regression - a new method based on robust nonlinear regression and the false discovery rate. *BMC Bioinformatics.* 2006;7(123.

FIGURE LEGENDS

Figure 1: Relationship between TCR dissociation rates and functional avidity of self/tumor- and virus-specific CD8 T cell clones. Correlations between EC_{50} values from (**A**) killing, (**B**) CD107a degranulation, (**C**) IFNγ-, (**D**) TNFα- and (**E**) IL-2-production titration assays and NTAmer-derived TCR dissociation rates (k_{off}). (**F**) Correlations between percentages of proliferating cells upon antigen-specific stimulation and NTAmer-derived TCR dissociation rates (k_{off}). (**A-F**) Antigen-specific CD8 T cell clones were generated upon direct ex vivo sorting from effector-memory (EM)/$CD28^{+/-}$ and/or EMRA/$CD28^{-}$ subsets. Each data point represents an A2/Melan-A_{26-35}- (derived from patient LAU618, ○), A2/NY-ESO-$1_{157-165}$- (patient LAU155, □), A2/$pp65_{495-504}$- or A2/$BMFL1_{259-267}$- (healthy donor BCL4, ◇) specific individual T cell clone. Non-functional clones are represented in grey boxes. The number of clones displaying function *n*, as well as Spearman's correlation (two tailed, $\alpha = 0.05$) coefficients *R* and *p* values are indicated. Color-coded and black lines are indicative of regression fitting and 95% confidence intervals, respectively. Of note, only very low numbers of outliers were identified when applying the ROUT method and are highlighted in color (71). The representative TCR-BV-CDR3 clonotype diversity of each antigenic specificity was; LAU618/Melan-A, 77%; LAU155/NY-ESO-1, 43%; BCL4/pp65, 57%; BCL4/BMFL1, 67%.

Figure 2: Relationship between TCR dissociation rates and polyfunctionality of self/tumor- and virus-specific CD8 T cell clones. (**A**) CD107a, IFNγ, TNFα and IL-2 co-expression titration assays of A2/Melan-A_{26-35}- (derived from patient LAU618), A2/NY-ESO-$1_{157-165}$- (patient LAU155), A2/$pp65_{495-504}$- or A2/$BMFL1_{259-267}$- (healthy donor BCL4) specific clones with slow (n = 10) or fast (n = 10) TCR off-rates. Pie arcs depict the average

fraction of cells displaying 0 to 4 functions. (**B**-**C**) Individual and (**D**) average ± SEM polyfunctional (co-expression of CD107a, IFNγ, TNFα and IL-2) titration curves obtained for A2/Melan-A_{26-35}- (derived from patient LAU618), A2/NY-ESO-$1_{157-165}$- (patient LAU155), A2/$pp65_{495-504}$- or A2/$BMFL1_{259-267}$- (healthy donor BCL4) specific clones with slow (n = 10, plain symbols and solid lines) or fast (n = 10, empty symbols and dotted lines) TCR off-rates Vertical lines indicated EC_{50} values. The *p* values were determined by the extra sum-of-squares F-test (α = 0.05). The representative TCR-BV-CDR3 clonotype diversity of each antigenic specificity was; LAU618/Melan-A, 80%; LAU155/NY-ESO-1, 45%; BCL4/pp65, 65%; BCL4/BMFL1, 80%.

Figure 3: Relationship between TCR dissociation rates and activating/inhibitory receptor expression of self/tumor- and virus-specific CD8 T cell clones. Correlations between fold increases in surface expression of (**A**) CD28, (**B**) CD137, (**C**) LAG-3, (**D**) PD-1, (**E**) TIGIT and (**F**) TIM-3 upon antigen-specific stimulation and NTAmer-derived TCR dissociation rates (k_{off}). (**G**) Correlations between baseline surface expression levels (gMFI) of CD5 and NTAmer-derived TCR dissociation rates (k_{off}). (**A-G**) Each data point represents an A2/Melan-A_{26-35}- (derived from patient LAU618, ○), A2/NY-ESO-$1_{157-165}$- (patient LAU155, □), A2/$pp65_{495-504}$- or A2/$BMFL1_{259-267}$- (healthy donor BCL4, ◇) specific individual T cell clone. The number of clones tested *n*, as well as Spearman's correlation (two tailed, α = 0.05) coefficients *R* and *p* values are indicated. Color-coded and black lines are indicative of regression fitting and 95% confidence intervals, respectively. Outliers were determined by the ROUT method and are highlighted in color (71). The representative TCR-BV-CDR3 clonotype diversity of each antigenic specificity was; LAU618/Melan-A, 77%; LAU155/NY-ESO-1, 43%; BCL4/pp65, 57%; BCL4/BMFL1, 67%.

Figure 4: Relationship between TCR dissociation rates and tumor control in immunodeficient mice upon adoptive T cell transfer. (A) Individual or (**B**) average ± SEM tumor growth and (**C**) Kaplan–Meier survival curves of tumor bearing NSG mice adoptively transferred with PBS (control, n = 7; black solid lines) or $1x10^6$ A2/Melan-A_{26-35}-specific T cell clones with fast (n = 4; blue dotted lines) or slow (n = 7; blue solid lines) TCR off-rates. (**D)** Individual or (**E**) average ± SEM tumor growth curves of tumor bearing NSG mice adoptively transferred with two-times $1x10^6$ A2/NY-ESO-$1_{157-165}$-specific T cell clones with fast (n = 5; green dotted lines) or slow (n = 5; green solid lines) TCR off-rates. Tumor volume and survival curves *p* values were determined by two-way-ANOVA and log-rank tests, respectively. (**F**) Representative staining and (**G**) absolute counts of human CD8 T cells from blood taken from tail veins at day 2 following adoptive transfer of $4x10^6$ A2/NY-ESO-$1_{157-165}$-specific CD8 T cell clones with fast (n = 4; green empty circles) or slow (n = 3; green full circles) TCR off-rates. As control, three mice received PBS (n = 4; black squares). *p* values were determined by one-way ANOVA multiple comparison tests.

Figure 5: TCR dissociation rates according to the antigenic specificity, clonotype repertoire and ex vivo differentiation status of CD8 T cell clones. (A, B) NTAmer-derived TCR dissociation rates (k_{off}) of EM/EMRA $CD28^{+/-}$ clones (n = 414) specific for the differentiation antigen A2/Melan-A_{26-35} (derived from melanoma patients LAU618, LAU627 and LAU818 following vaccination with Melan-A/peptide, IFA and CpG), the cancer testis A2/NY-ESO-$1_{157-165}$ (from patients LAU50 and LAU155 with naturally occurring T cell responses) or the persistent herpes viruses A2/$pp65_{495-504}$ or A2/$BMFL1_{259-267}$ (from healthy donors BCL4 and BCL6), categorized according to (**A**) the respective patients and donors or

(**B**) antigenic specificity. (**C**) NTAmer-derived TCR dissociation rates (k_{off}) of individual TCR-BV-CDR3 clonotypes specific for the tumor epitopes A2/Melan-A_{26-35} (n = 27) and A2/NY-ESO-$1_{157-165}$ (n = 24), and the persistent herpes virus epitopes A2/$pp65_{495-504}$ (n = 37) and A2/$BMFL1_{259-267}$ (n = 55). (**D**) NTAmer-derived TCR dissociation rates (k_{off}) of A2/Melan-A_{26-35}-specific clones derived from HLA-A2-negative (HD1 and HD2), HLA-A2-positive (HD3 and HD4) healthy donors, HLA-A2-positive unvaccinated (LAU975 and LAU1013) and A2/Melan-A_{26-35}-vaccinated (LAU618, LAU627 and LAU818) melanoma patients, categorized according to the patient/donor groups and the differentiation status of T cell clones. (**A-D**) Data are depicted as box (25^{th} to 75^{th} percentiles) and whisker (10^{th} to 90^{th} percentiles) with the middle line representing the median. Numbers of clones *n*, as well as Kruskal-Wallis test ($\alpha = 0.05$) derived *p* values are indicated. Significant differences between the A2/Melan-A_{26-35}- and the A2/NY-ESO-$1_{157-165}$-specific groups were obtained by Mann Whitney test (two tailed).

Figure 6: Inter-experimental and over-time variations of TCR dissociation rates, pMHC multimer staining and functional avidity assays. (**A**) NTAmer-derived TCR dissociation rates (k_{off}), (**B**) NTAmer surface staining levels (gMFI) and (**C**) killing avidity values (EC_{50}) obtained in independent assays (n > 4) for A2/Melan-A_{26-35}-specific CD8 T cell clones with slow (n = 6, plain symbols and solid lines) or fast (n = 6, empty symbols and dotted lines) TCR off-rates. (**A-C**) Data are depicted as individual values and box (minimum to maximum, with the middle line representing the mean). (**D**) NTAmer-derived TCR dissociation rates (k_{off}), (**E**) killing avidity values (EC_{50}) and (**F**) surface staining levels (gMFI) obtained over time (D10/11, D15 and D20/21; D = day) following non-specific stimulation (by PHA and irradiated feeder cells) for A2/Melan-A_{26-35}-specific T cell clones with slow (n = 6, plain symbols and solid lines) or fast (n = 6, empty symbols and dotted lines) TCR off-rates. S2

represents the off-rate measurements of the same clones six months before the 5th round of stimulation (S5). The *p* values were determined by the Friedman ($\alpha = 0.05$) and Wilcoxon matched-pair signed rank (two tailed) tests.

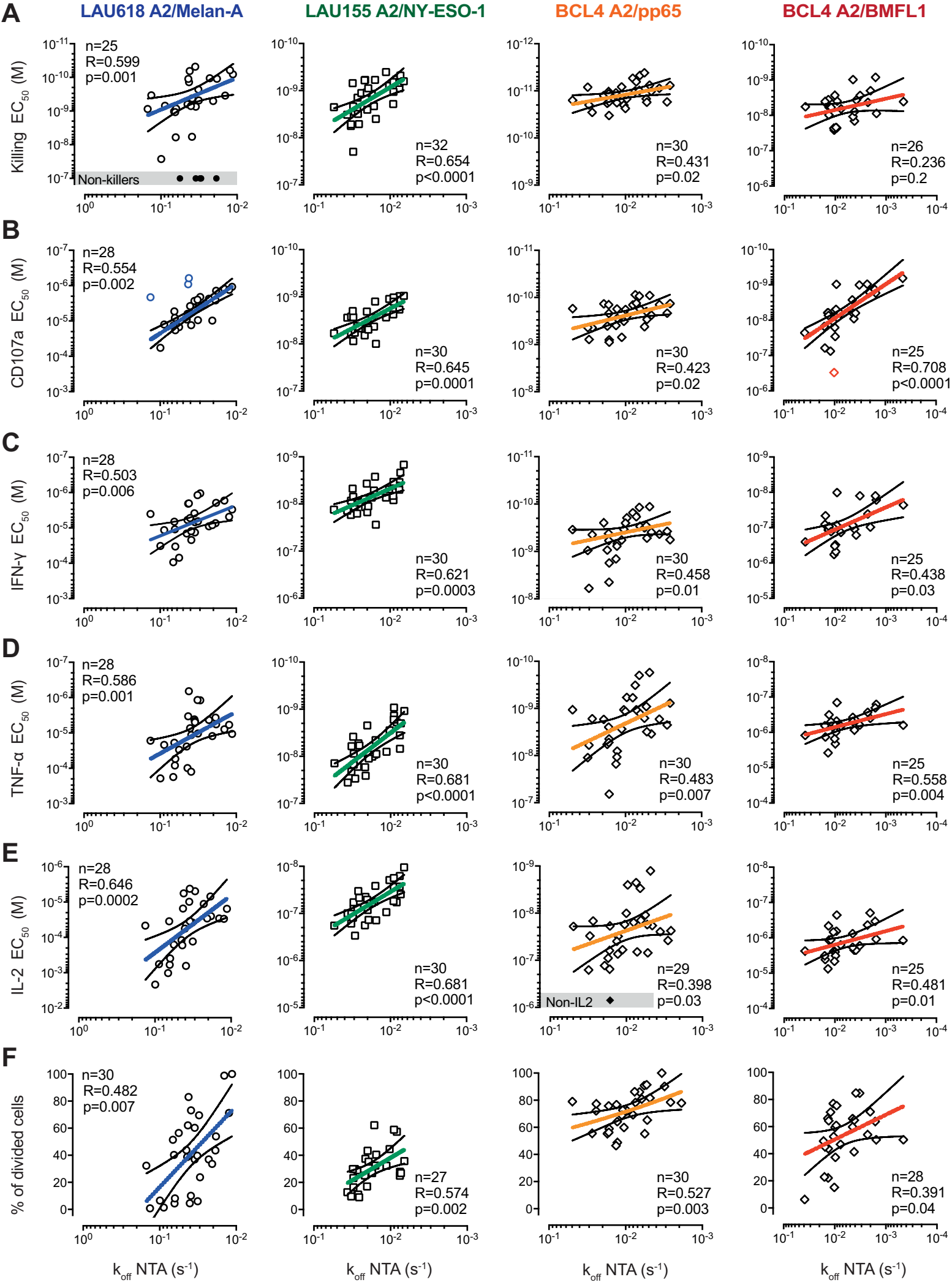

Figure 1 - Allard et al.

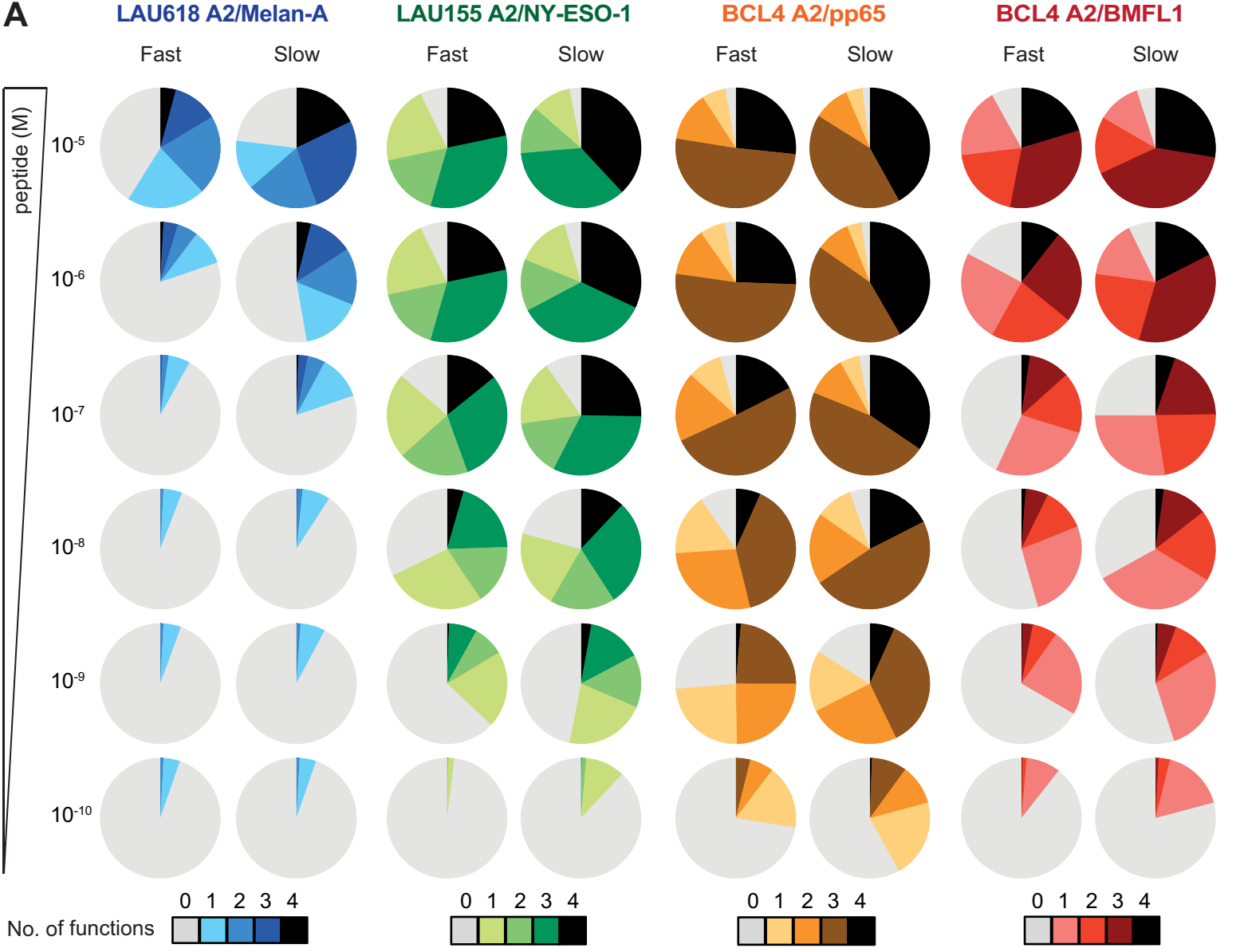

Figure 2 - Allard et al.

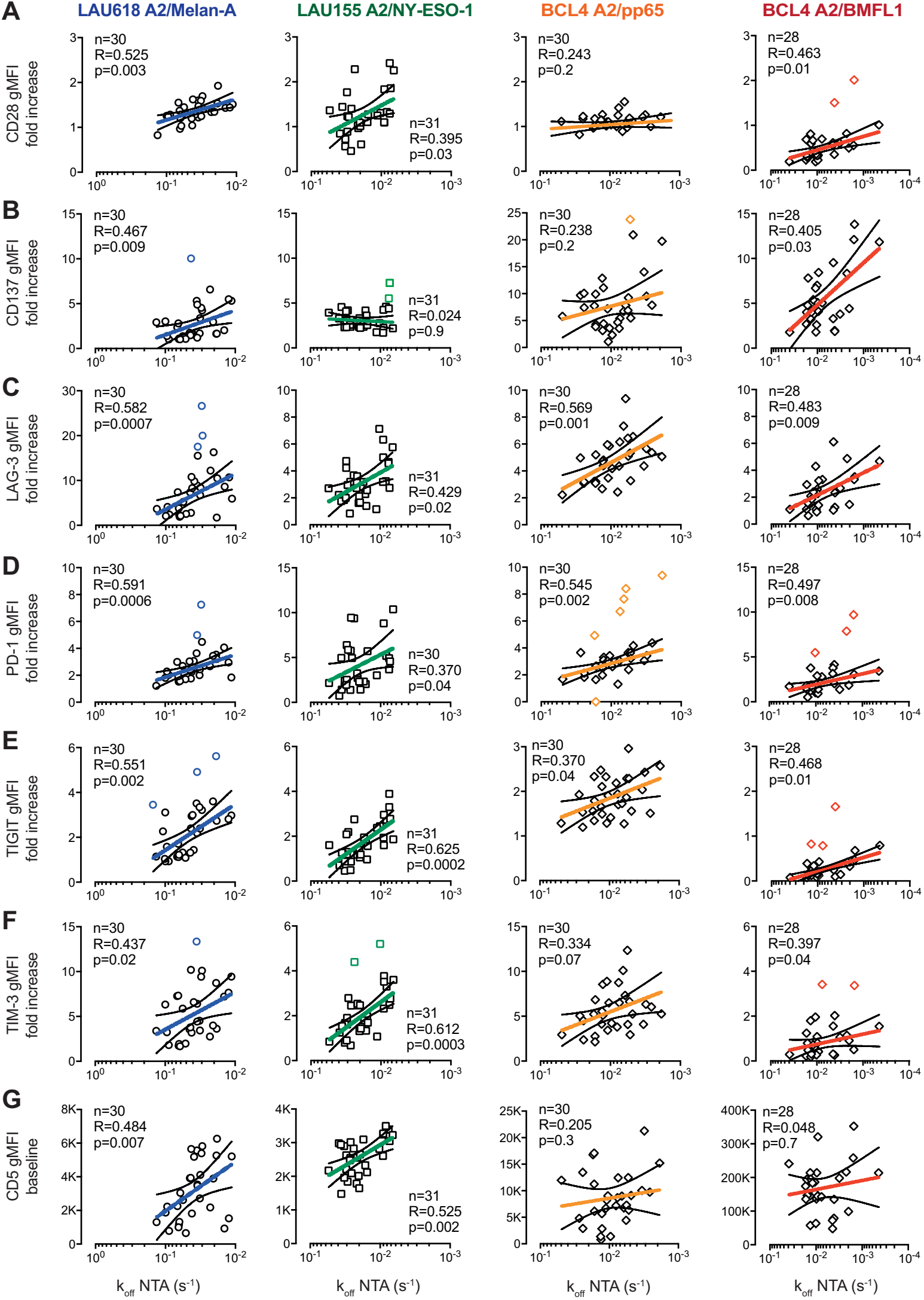

Figure 3 - Allard et al.

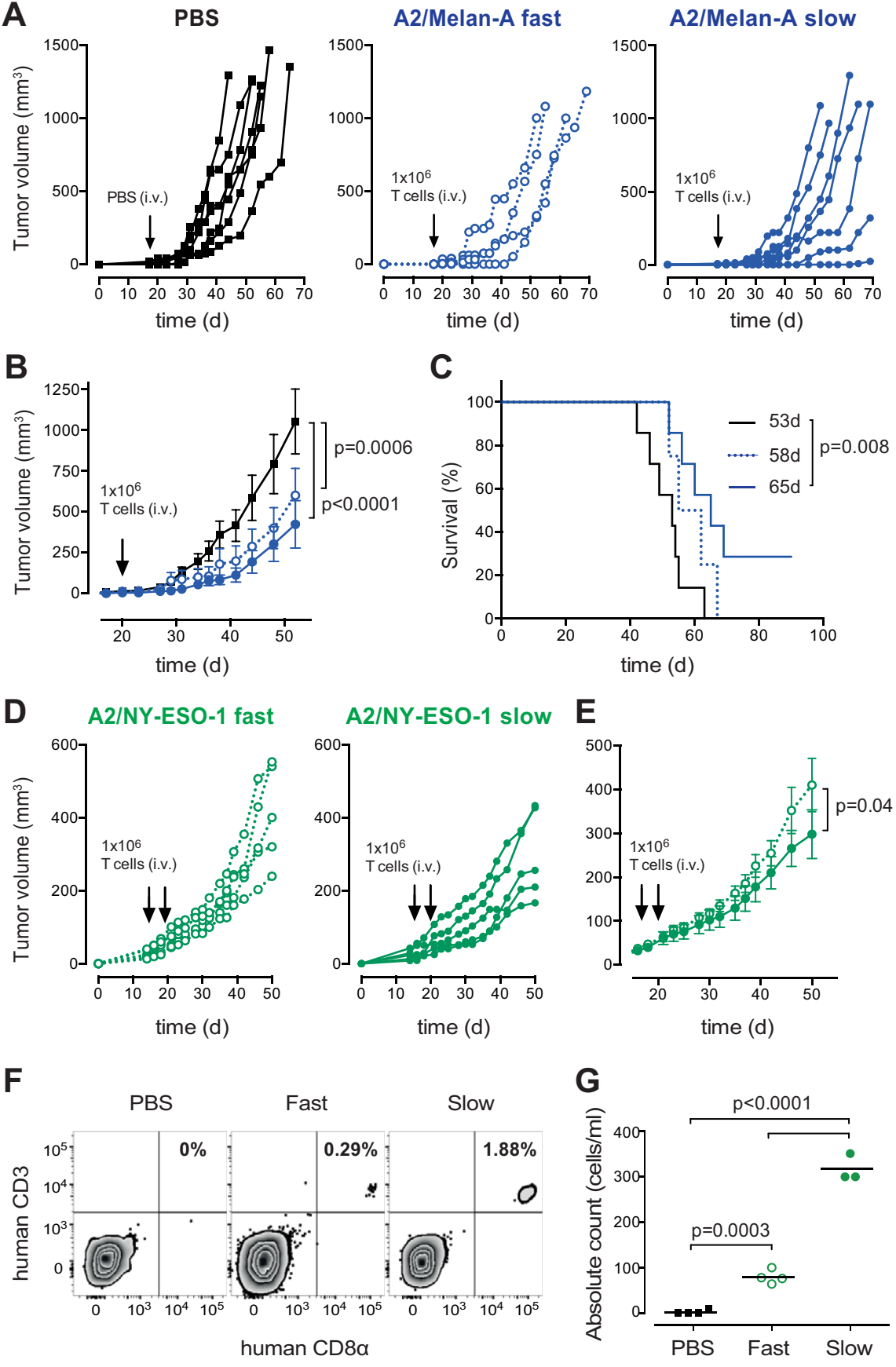

Figure 4 - Allard et al.

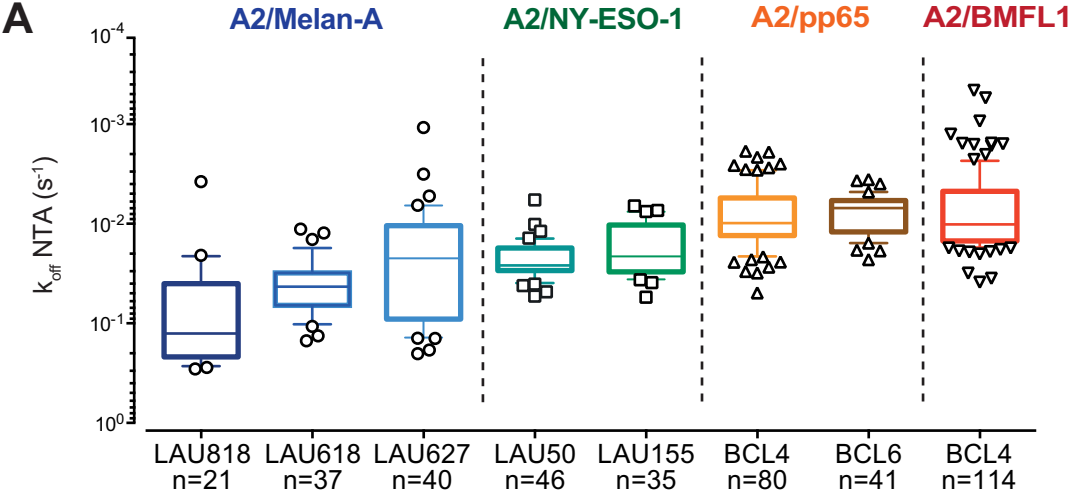

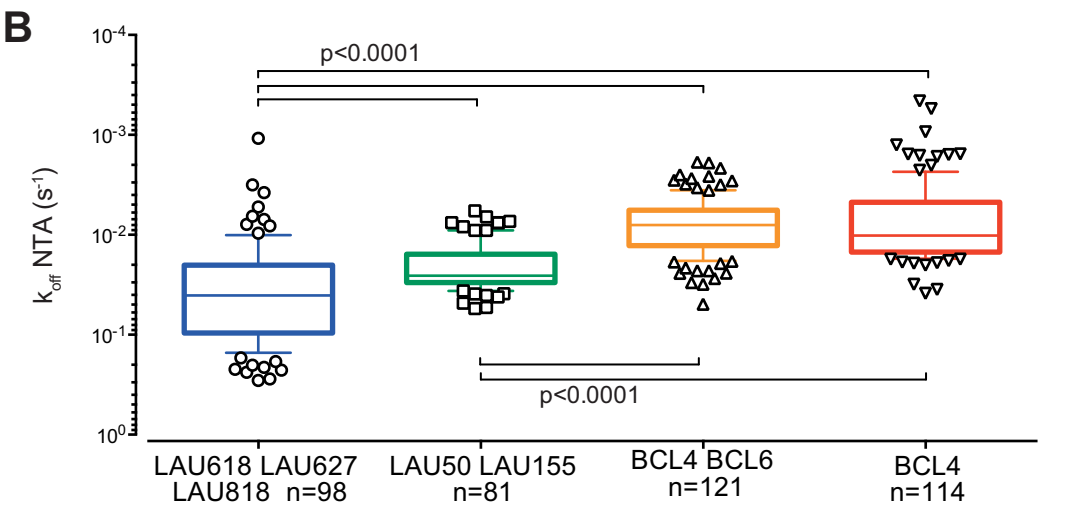

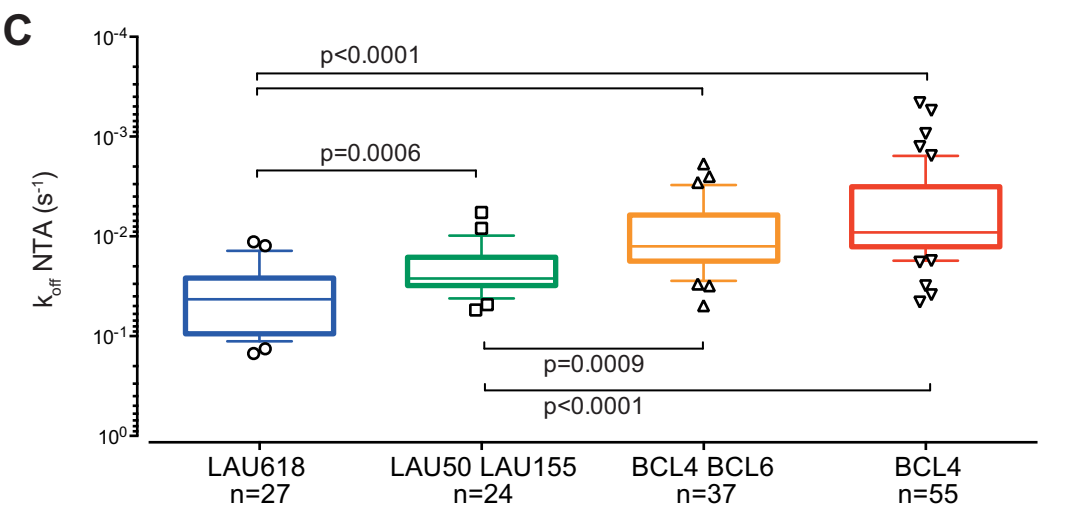

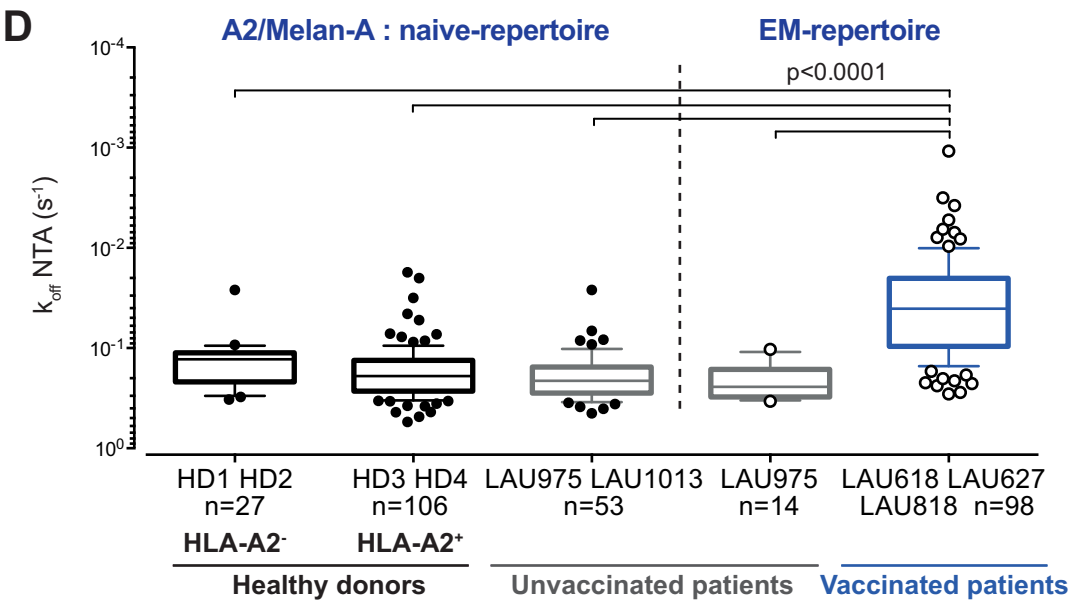

Figure 5 - Allard et al.

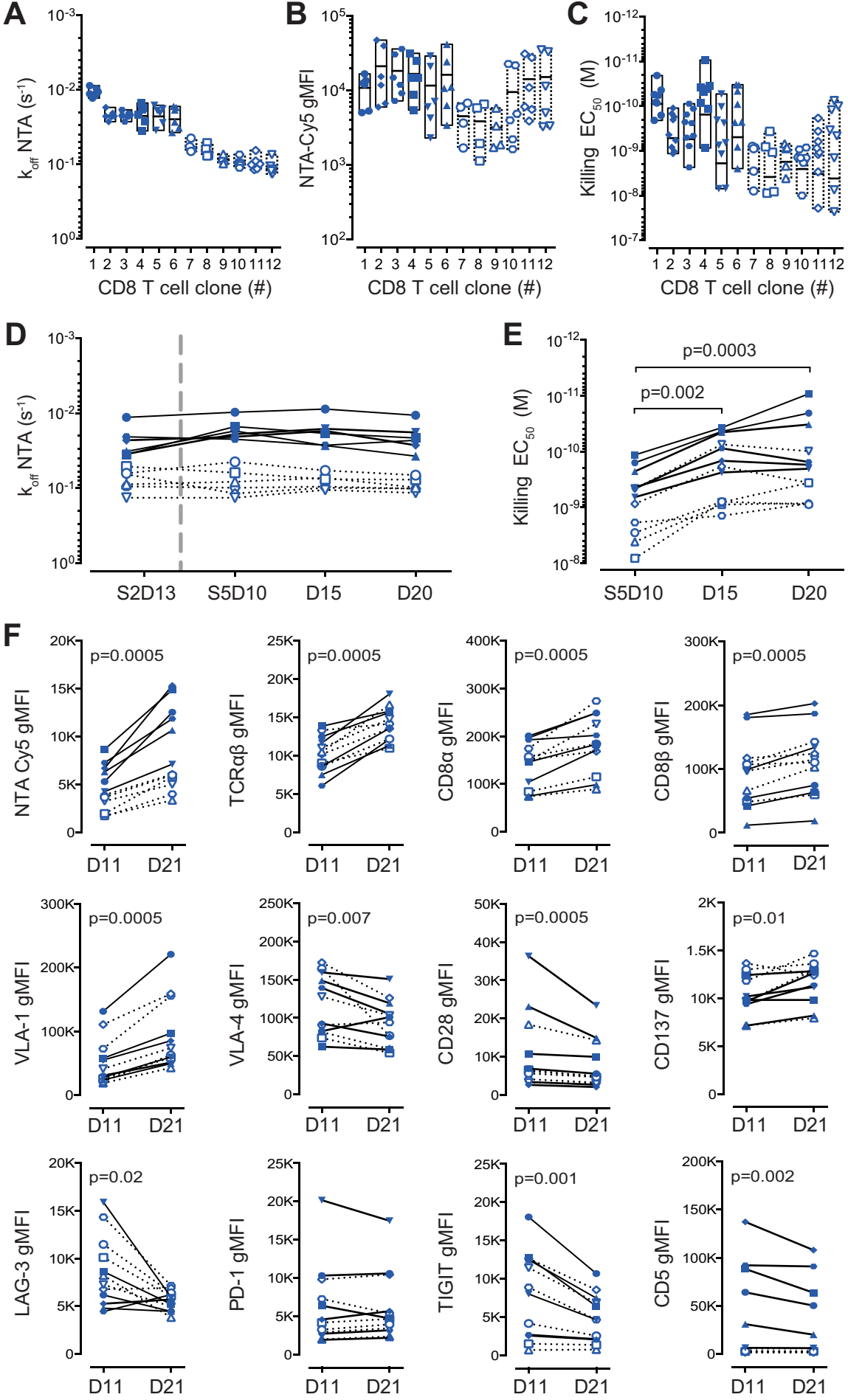

Figure 6 - Allard et al.

SUPPLEMENTAL MATERIALS

Supplemental Table 1. List of TCR-BV-CDR3 clonotypes and their off-rate values.

Antigenic specificity	Patient/ Donor	Clonotype	BV family	CDR3 (amino acids)	BJ	Mean koff (s-1)
A2/Melan-A	LAU618	clono 1	BV3	SPPGLSGNIQ	2.4	0.03338
		clono 2	BV3	SFQGVGTGEL	2.2	0.02622
		clono 3	BV13	SYGPLSGAGY	1.2	0.02548
		clono 4	BV13	SPGTLADTQ	2.3	0.06173
		clono 5	BV13	SAGYGQPQ	1.5	0.05155
		clono 6	BV14	RAGALQGEQ	2.7	0.10740
		clono 7	BV14	SPAALSGAYEQ	2.7	0.10100
		clono 8	BV17	SPGALNTEA	1.1	0.06438
		clono 9	BV3	SFPRWGRNYSYNEQ	na	0.03492
		clono 10	BV14	SLSAGTGVLDTQ	na	0.09449
		clono 11	BV17	SIGA--EHEQ	na	0.09964
		clono 12	BV17	SIEALQGFTEA	na	0.04187
		clono 13	BV17	RWGVLNTEA	na	0.01835
A2/NY-ESO-1	LAU155	clono 1	BV1	SVATGGDTQ	2.3	0.01875
		clono 2	BV8	NSGSNEQ	2.1	0.02771
		clono 3	BV8	SLGSTEA	1.1	0.00831
		clono 4	BV8	NSGANEQ	2.1	0.02026
		clono 5	BV8	RKGPNEQ	2.1	0.03529
		clono 6	BV13	SYVGAAGEL	2.2	0.02918
		clono 7	BV13	SLTGGLNSPL	na	0.03146
		clono 8	BV1	SLATGEDTQ	na	0.01574
		clono 9	BV13	LGDGDGAYNSPL	1.6	0.03277
	LAU50	clono 10	BV8	QQGGTEA	1.1	0.01572
		clono 11	BV8	SLGGTEA	1.1	0.01975
		clono 12	BV13	RTGLDGY	1.2	0.03094
		clono 13	BV13	SYVGGKAEA	1.2	0.02612
A2/CMV-pp65	BCL4	clono 1	BV1	SVYGGAGNSPL	1.6	0.00866
		clono 2	BV1	SYPGGNTI	1.3	0.01797
		clono 3	BV3	SFLGYTEA	1.1	0.01174
		clono 4	BV8	SSVNEA	1.1	0.00646
		clono 5	BV8	SSAGGAVYGY	1.2	0.02039
		clono 6	BV9	SLLLGTAAEA	1.1	0.00313
		clono 7	BV14	RLLAGGRSAQ	2.5	0.00608
		clono 8	BV3	SFSSPGQGSTDTQ	2.3	0.01285
		clono 9	BV8	SSVLEA	1.1	0.01002
		clono 10	BV8	SLVGGVDGY	1.2	0.03013
		clono 11	BV8	SIMDYGY	1.2	0.03125
		clono 12	BV13	SAVTGAVDQPQ	1.5	0.01642
		clono 13	BV13	SYFYYEQ	2.7	0.00251
		clono 14	BV13	SYSTGTAYGY	1.2	0.00289
		clono 15	BV13	SPKTGVPYEQ	2.7	0.02146
	BCL6	clono 16	BV8	SSANYGY	1.2	0.01505
		clono 17	BV13	SRQTGAAYGY	1.2	0.00617
		clono 18	BV13	SYATGTAYGY	1.2	0.00530
A2/EBV-BMFL1	BCL4	clono 1	BV2	RDRTGNGY	1.2	0.005131
		clono 2	BV2	RDSVGNGY	1.2	0.002706
		clono 3	BV2	RDRVGNGY	1.2	0.001934
		clono 4	BV2	RDSTGNGY	1.2	0.004689
		clono 5	BV2	RVEPGNGY	1.2	0.009871
		clono 6	BV4	VGTGGTNEKL	1.4	0.014417
		clono 7	BV4	VGYGGTNEKL	1.4	0.013503
		clono 8	BV4	VGSGGTNEKL	1.4	0.045620
		clono 9	BV16	SQSPGGTQ	2.5	0.009123
		clono 10	BV16	SQSPGGEA	1.1	0.003469
		clono 11	BV16	SQSPGGTS	na	0.003878
		clono 12	BV18	SPPAVSYEQ	2.7	0.016529
		clono 13	BV2	DGY	1.2	0.017560

Supplemental Table 2. List of antibodies used in this study.

Name	Company	Catalog no	Clone no
APC anti-CD28	BD Pharmigen	559770	CD28.2
FITC anti-CD45RA	BD Pharmigen	561882	HI100
FITC anti-CD107a	BD Pharmigen	555800	H4A3
PerCPCy5.5 anti-IL2	BD Pharmigen	560708	MQ1-17H12
APC anti-IL13	BD Pharmigen	561162	JES10-5A2
PE-Cy7 anti-IFNγ	BD Pharmigen	557844	4S.B3
A700 anti-TNFα	BD Pharmigen	557996	MAb11
PE-Cy7 anti-CD5	BD Pharmigen	348810	L17F12
APC anti-CD137	BD Pharmigen	550890	4B4-1
PE anti-VLA-1	BD Pharmigen	559596	SR84
APC anti-VLA-4	BD Pharmigen	561794	MAR4 .
BrV421 anti-PD1	BD Pharmigen	562516	EH12.1
APC-A750 anti-CD8	Beckman Coulter	A94683	B9.11
Pacific-blue anti-CD8	Beckman Coulter	A82791	B9.11
FITC anti-CD8beta	Beckman Coulter	IM2217U	2ST8.5H7
PE-Cy7 anti-CD8alpha	Beckman Coulter	737661	SFCI21Thy2D3
PE anti-pan-TCRab	Beckman Coulter	A39499	IP26A
PE-Cy7 anti-CCR7	Biolegend	353226	G043H7
PE anti-IL4	Biolegend	500810	MP4-25D2
BrV421 anti-CD28	Biolegend	302930	CD28.2
A488 anti-PD1	AbD Serotech	MCA2628A488	MIH4
APC anti-TIGIT	eBioscience	17-9500-42	MBSA43
FITC anti-LAG-3	Enzo	ALX-804-806F-C100	17B4
PE anti-TIM-3	R&D systems	FAB2365P	344823

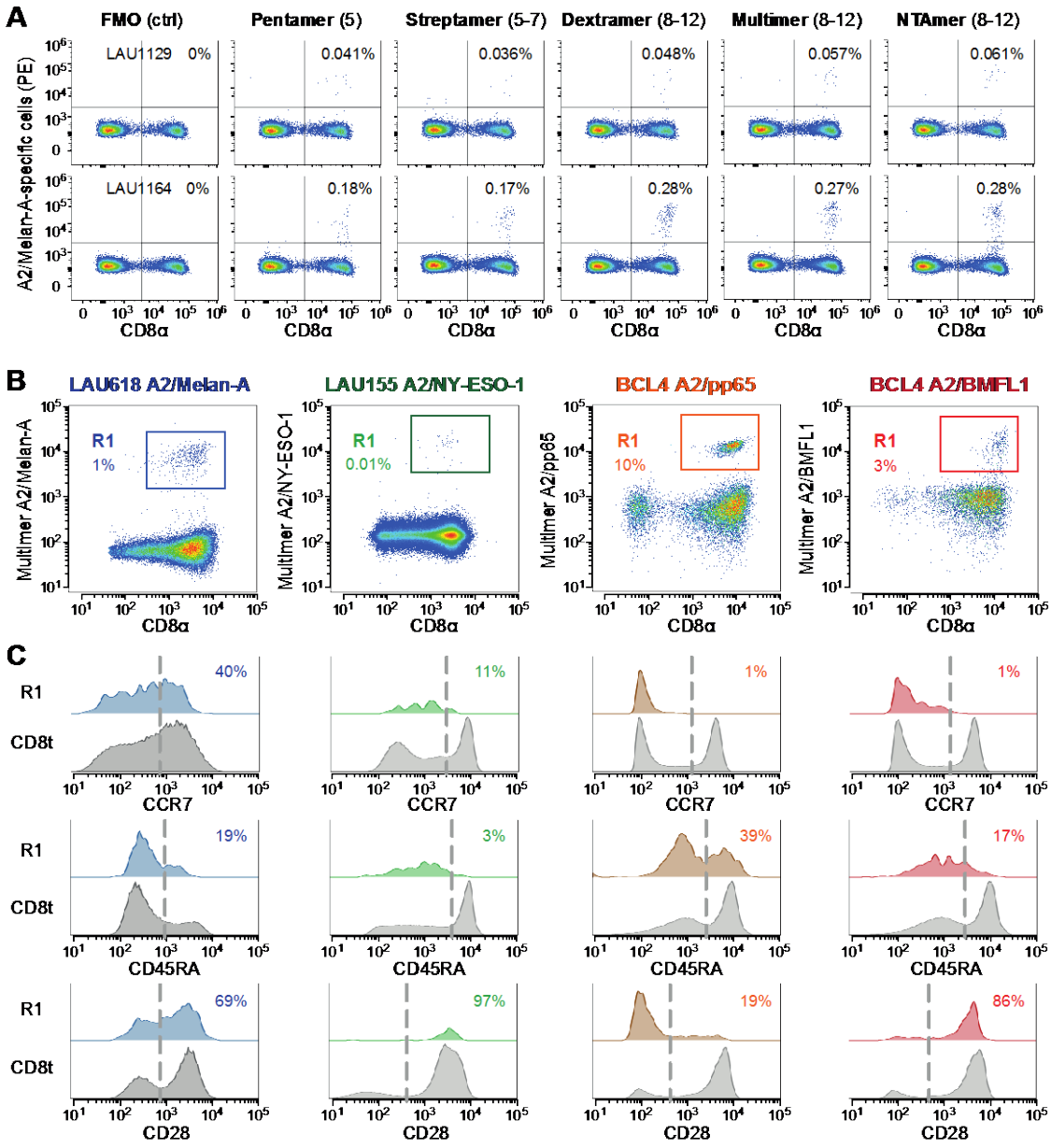

Sup Figure 1 - Allard et al.

Supplemental Figure 1: Ex vivo detection of antigen-specific CD8 T cells using pMHC-based reagents and analysis of blood samples used to generate self/tumor- and virus-specific CD8 T cell clones. (A) Comparison of A2/MelanA$_{26-35}$-specific staining from PBMCs obtained from melanoma patients (LAU1129 and LAU1164) using PE-labeled pentamers, streptamers, multimers and NTAmers. Gating was done on live CD14-/CD16-/CD19-/CD3+ lymphocytes. The valence of pMHC reagents is indicated in brackets, as well as percentages of positively stained cells. FMO (fluorescence minus one). (**B**) CD8 and multimer staining of CD8-enriched PBMCs from melanoma patients LAU618 (A2/Melan-A$_{26-35}$), LAU155 (A2/NY-ESO-1$_{157-165}$) and healthy donor BCL4 (A2/pp65$_{495-504}$ or A2/BMFL1$_{259-267}$). (**C**) CCR7, CD45RA and CD28 staining of the corresponding multimer-

specific (*R1*) and total CD8 T cell (*CD8t*) populations. Percentages of positively stained cells are indicated. Melan-A/specific CD8 T cell clones (from patient LAU618) exhibited an EM/CD28$^{+/-}$ phenotype, while NY-ESO-1-specific T cell clones (from patient LAU155) presented mostly an early-differentiated EM/CD28^{+} phenotype. EBV/BMFL1-specific CD8 T cell clones were predominantly EM/CD28^{+}, whereas CMV/pp65-specific clones mostly exhibited a differentiated EMRA/CD28^{-} phenotype.

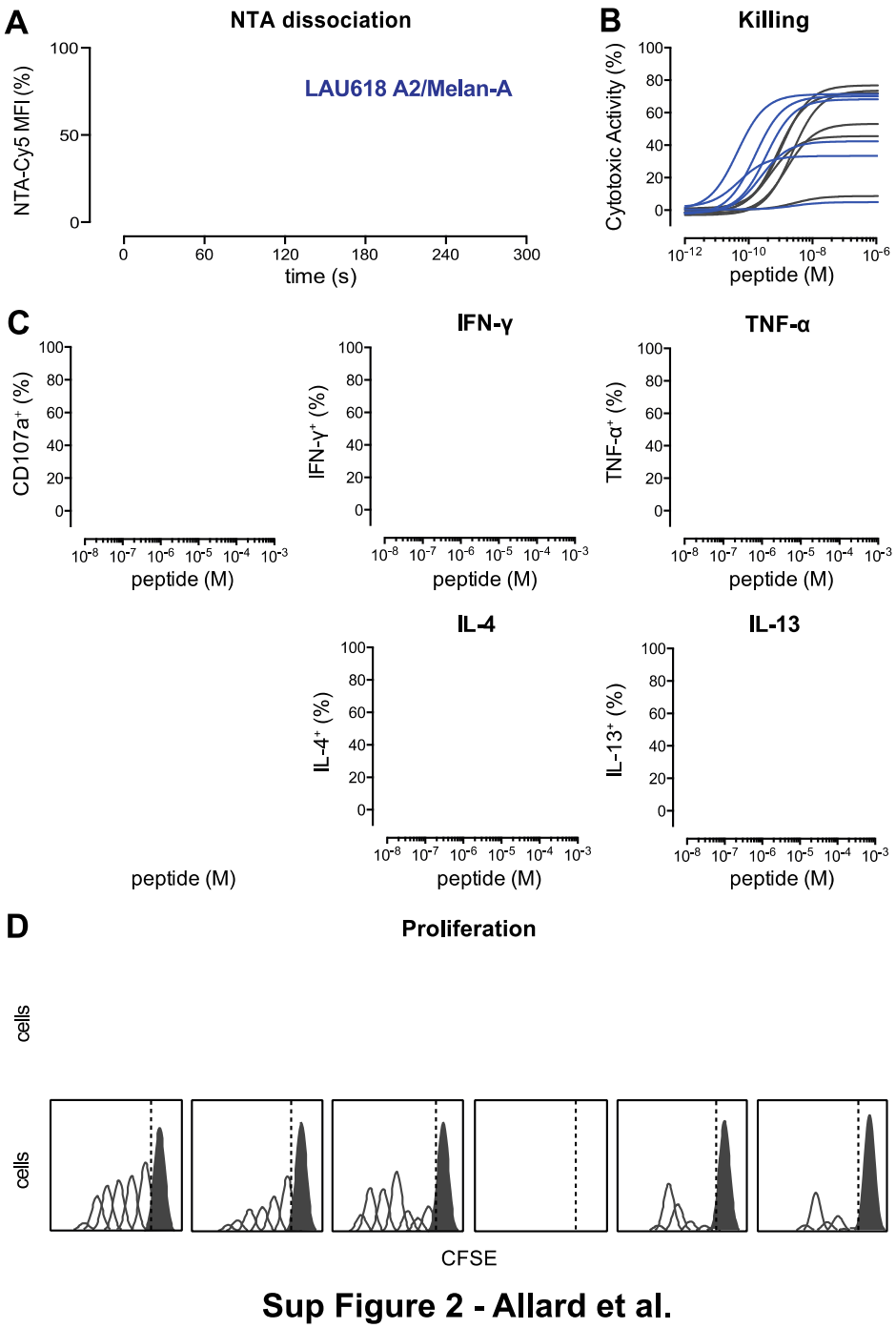

Sup Figure 2 - Allard et al.

Supplemental Figure 2: *In vitro* analysis of TCR dissociation-rates versus functional avidities of self/tumor- and virus-specific CD8 T cell clones. Representative (**A**) NTAmer-dissociation curves, (**B**) killing-, **(C)** CD107a degranulation-, IFNγ-, TNFα-, IL-2-, IL-4- and IL-13-production titration curves and **(D)** proliferation analysis (by CFSE fluorescence histograms) obtained for A2/Melan-A_{26-35}-specific CD8 T cell clones from patient LAU618, defined as slow (n = 6, blue lines) or fast (n = 6, grey lines) TCR off-rates. Non-divided and divided T cells are represented as plain and empty peaks, respectively.

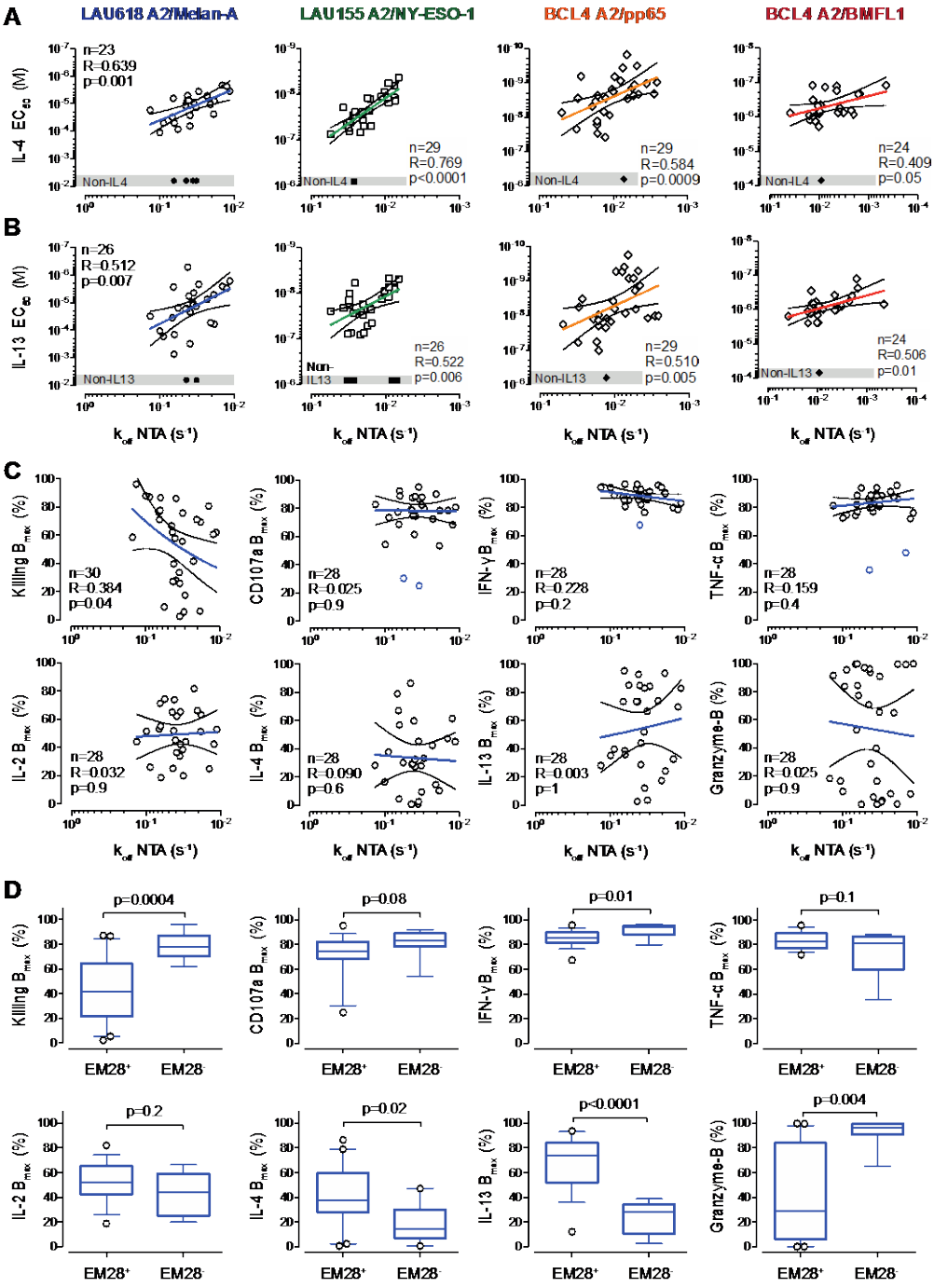

Sup Figure 3 - Allard et al.

Supplemental Figure 3: Relationship between TCR dissociation-rates, functional avidity and maximal function capacity of self/tumor- and virus-specific CD8 T cell clones. Correlations between EC_{50} values from (**A**) IL-4- and (**B**) IL-13-production titration assays, and NTAmer-derived TCR dissociation-rates (k_{off}). (**C**) Correlations between B_{max} values from killing, CD107a-degranulation, IFNγ-, TNFα-, IL-2-, IL-4- and IL-13-production titration assays, or percentages of granzyme-B expressing T cells, and NTAmer-derived TCR dissociation-rates (k_{off}). (**A-C**) Each data-point represents an A2/Melan-A_{26-35}- (derived from patient LAU618, ○), A2/NY-ESO-$1_{157-165}$- (patient LAU155, □), A2/$pp65_{495-504}$- or

A2/BMFL1$_{259-267}$- (healthy donor BCL4, ◇) specific individual T cell clone. Non-functional clones are represented in grey boxes. The number of clones displaying function *n*, as well as Spearman's correlation (two tailed, $\alpha = 0.05$) coefficient *R* and *p* values are indicated. Color-coded and black lines are indicative of regression fitting and 95% confidence intervals, respectively. (**D**) B_{max} values from killing, CD107a-degranulation, IFNγ-, TNFα-, IL-2-, IL-4- and IL-13-production titration assays, or granzyme-B expression, of early-differentiated effector-memory EM/CD28$^+$ or late-differentiated EM/CD28$^-$ A2/Melan-A$_{26-35}$-specific T cell clones derived from patient LAU618. Data are depicted as box (25th to 75th percentiles) and whisker (10th to 90th percentiles) with the middle line representing the median. Numbers of clones *n*, as well as Mann-Whitney (two tailed) derived *p* values are indicated. Of note, upon high peptide-dose stimulation (at Bmax, maximal response), differentiated EM/CD28$^-$-derived CD8 T cell clones displayed higher granzyme-B expression, cytotoxic and IFN-γ production capacity, but a lower ability to produce IL-2, IL-4 or IL-13 than memory EM/CD28$^+$ T cells.

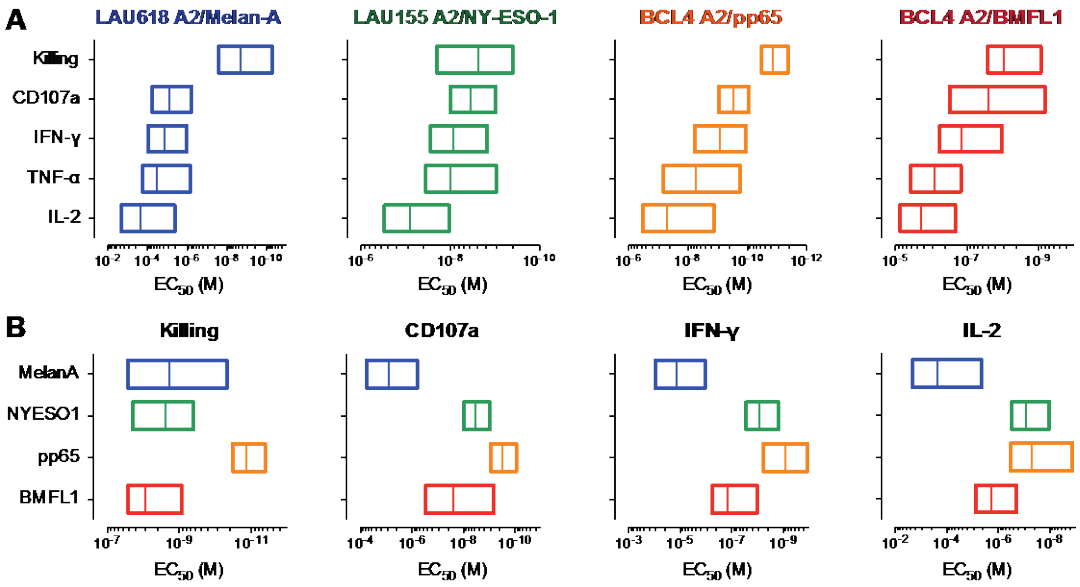

Sup Figure 4 - Allard et al.

Supplemental Figure 4: Functional avidities according to the functional assay or the antigenic specificity of CD8 T cell clones. Comparison of functional avidity (EC_{50}) from killing-, CD107a degranulation-, IFNγ-, TNFα- and IL-2-production of A2/Melan-A_{26-35}- (derived from melanoma patient LAU618, n = 30), A2/NY-ESO-$1_{157-165}$- (patient LAU155, n = 32), A2/$pp65_{495-504}$- or A2/$BMFL1_{259-267}$- (healthy donor BCL4, n = 30 and 26, respectively) specific CD8 T cell clones classified according to (**A**) the functional assay and (**B**) the antigenic-specificity. Data are depicted as box (minimum to maximum) with the middle line representing the mean. The representative TCR-BV clonotype diversity of each antigenic specificity is as following; LAU618/Melan-A, 77%; LAU155/NY-ESO-1, 43%; BCL4/pp65, 57%; BCL4/BMFL1, 67%.

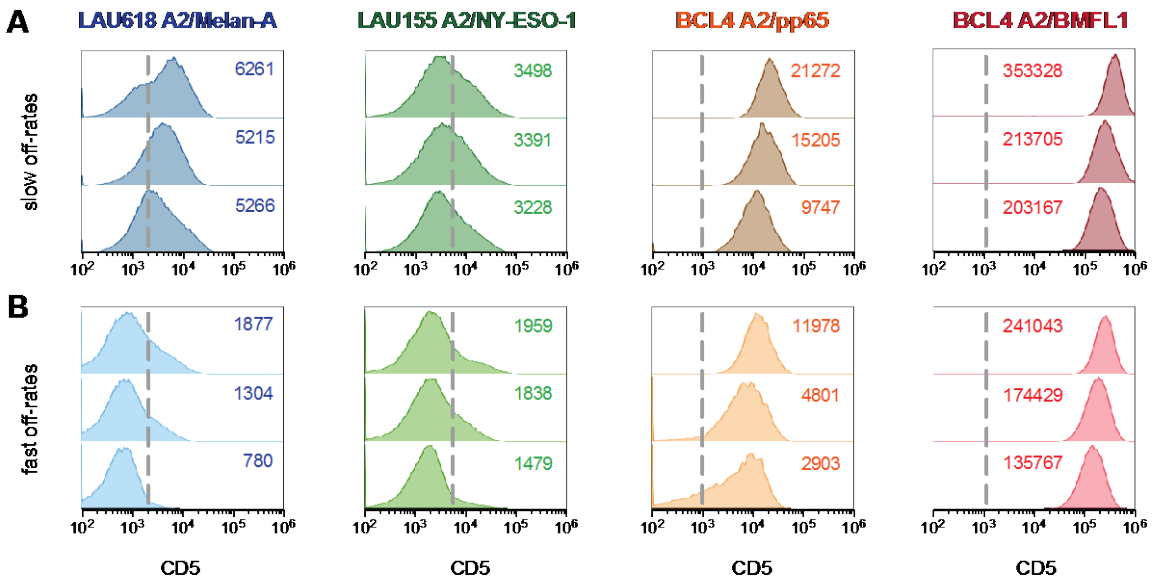

Sup Figure 5 - Allard et al.

Supplemental Figure 5: CD5 expression according to the TCR-dissociation off-rate parameter and antigenic specificity of self/tumor- and virus-specific CD8 T cell clones. CD5 surface staining was obtained at baseline (no antigen-specific stimulation) from representative antigen-specific CD8 T cells of (**A**) slow or (**B**) fast NTAmer-based off-rates. Data are depicted according to the antigenic specificity (A2/Melan-A_{26-35}-, A2/NY-ESO-$1_{157-165}$-, A2/$pp65_{495-504}$- and A2/$BMFL1_{259-267}$ antigens). Geometric fluorescence means (gMFI) are indicated.

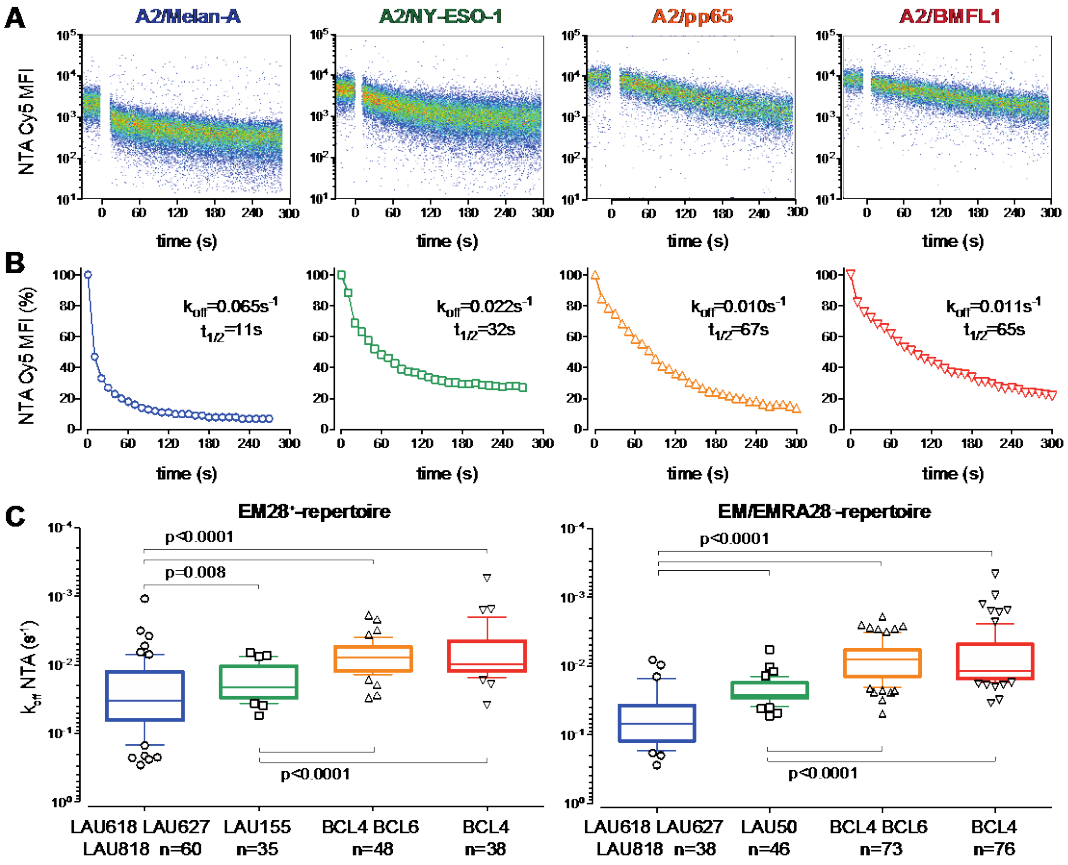

Sup Figure 6 - Allard et al.

Supplemental Figure 6: TCR dissociation-rates according to the antigenic specificity and *ex vivo* differentiation status. Representative (**A**) NTAmer-dissociation staining and (**B**) corresponding fitting curve obtained for A2/Melan-A_{26-35}- (○), A2/NY-ESO-$1_{157-165}$- (□), A2/$pp65_{495-504}$- (△) and A2/$BMFL1_{259-267}$- (▽) specific CD8 T cell clones, defined as average TCR off-rates. k_{off} and $t_{1/2}$ derived values are indicated. (**C**) NTAmer-derived TCR dissociation-rates (k_{off}) of early-differentiated effector-memory EM $CD28^+$ (left panel) versus late-differentiated EM/EMRA $CD28^-$ (right panel) clones specific for (i) A2/Melan-A_{26-35} (from vaccinated melanoma patients LAU618, LAU627 and LAU818), (ii) A2/NY-ESO-$1_{157-165}$ (from patients LAU50 and LAU155 with naturally occurring tumor-specific T cell responses) or (iii) the persistent herpes viruses A2/$pp65_{495-504}$ or A2/$BMFL1_{259-267}$ (from healthy donors BCL4 and BCL6), categorized according to their antigenic specificity. Data are depicted as box (25^{th} to 75^{th} percentiles) and whisker (10^{th} to 90^{th} percentiles), with the middle line representing the median. Antigen specificity is depicted according to specific colored codes and symbols. Numbers of clones *n*, as well as Kruskal-Wallis test ($\alpha = 0.05$) derived *p* values are indicated. Significant differences between the A2/Melan-A_{26-35}- and the A2/NY-ESO-$1_{157-165}$-specific groups were obtained by a Mann Whitney test (two tailed).

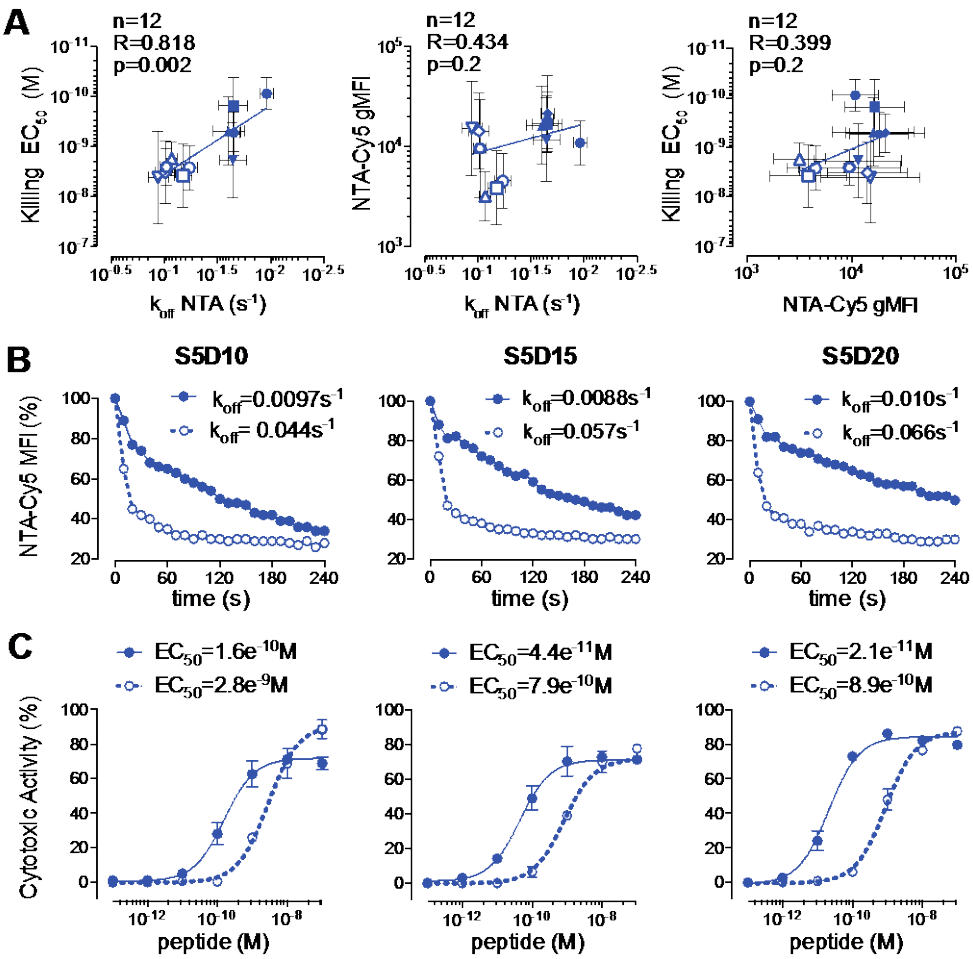

Sup Figure 7 - Allard et al.

Supplemental Figure 7: Correlations between TCR dissociation rates versus pMHC multimer staining versus functional avidity of CD8 T cell clones. (A) Correlations between NTAmer-derived TCR dissociation rates (k_{off}), NTAmer surface staining levels (gMFI) and killing avidity values (EC_{50}) obtained from independent assays (n = 4 to 9) for A2/Melan-A_{26-35}-specific CD8 T cell clones, defined as slow (n = 6, plain symbols) or fast (n = 6, empty symbols) TCR off-rates. Each symbol/clone is represented as average ± SD. The number of clones (n), as well as Spearman's correlation (two tailed, $\alpha = 0.05$) coefficients *R* and *p* values are indicated. Lines are indicative of linear regression fitting. Representative (**B**) NTAmer-dissociation and (**C**) killing-titration curves obtained at day 10 (D10), 15 (D15) and 20 (D20) following non-specific stimulation (by PHA and irradiated feeder cells) of A2/Melan-A_{26-35}-specific CD8 T cell clones, defined as slow (n =6, plain symbols and solid lines) or fast (n = 6, empty symbols and dotted lines) TCR off-rates. Average and SD percentages are depicted, as well as the corresponding fitting curves and k_{off} or EC_{50} derived values.

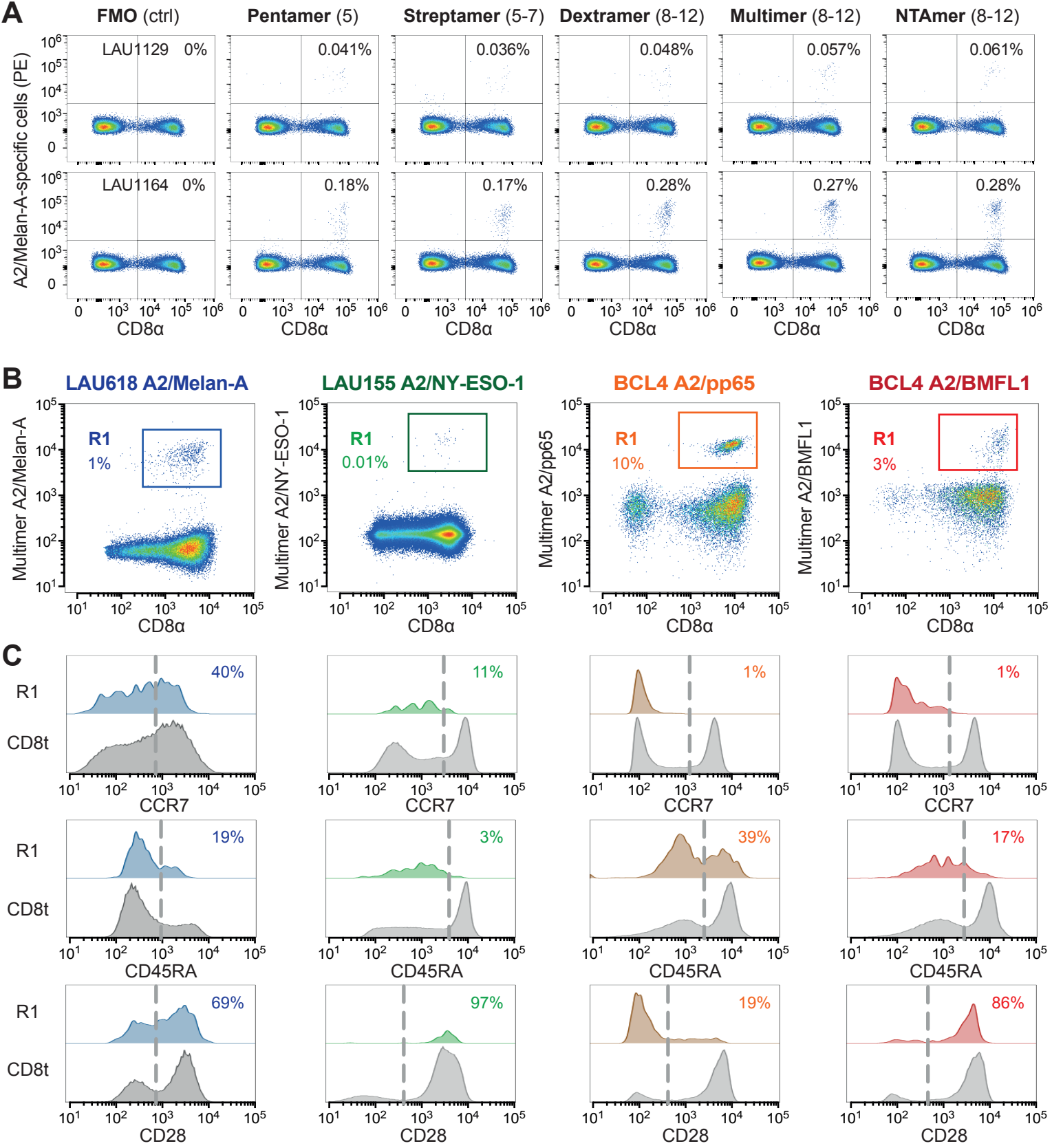

Sup Figure 1 - Allard et al.

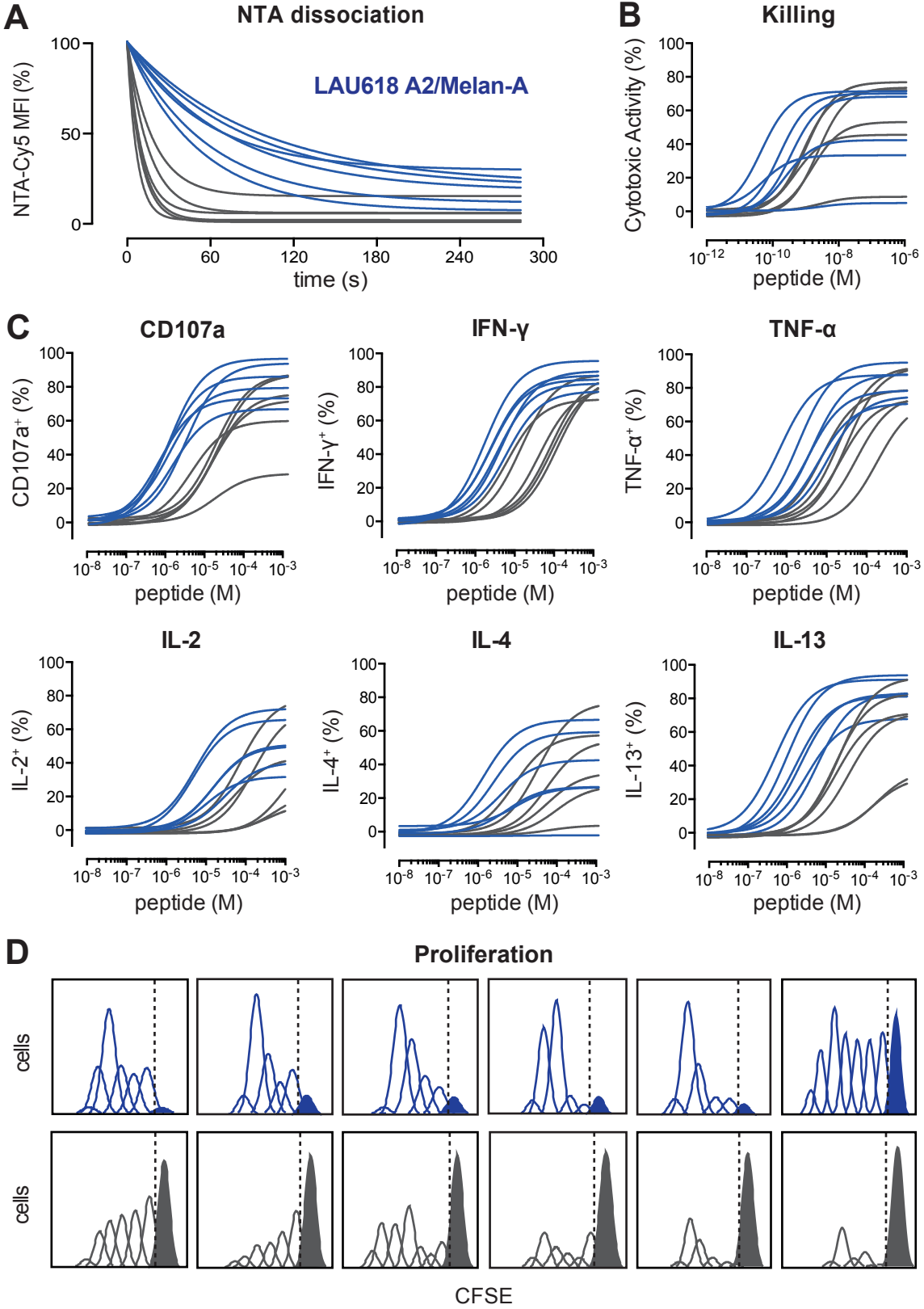

Sup Figure 2 - Allard et al.

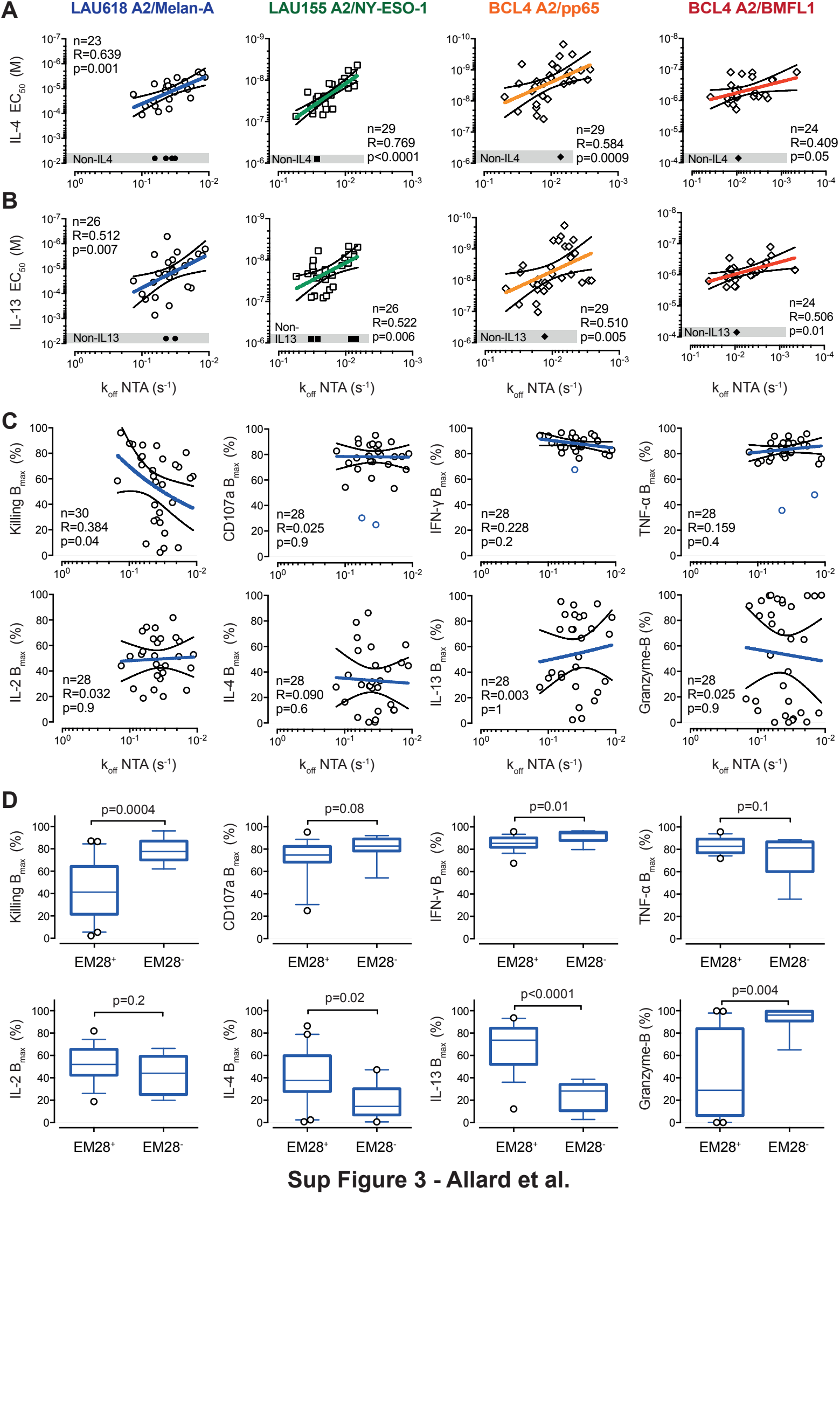

Sup Figure 3 - Allard et al.

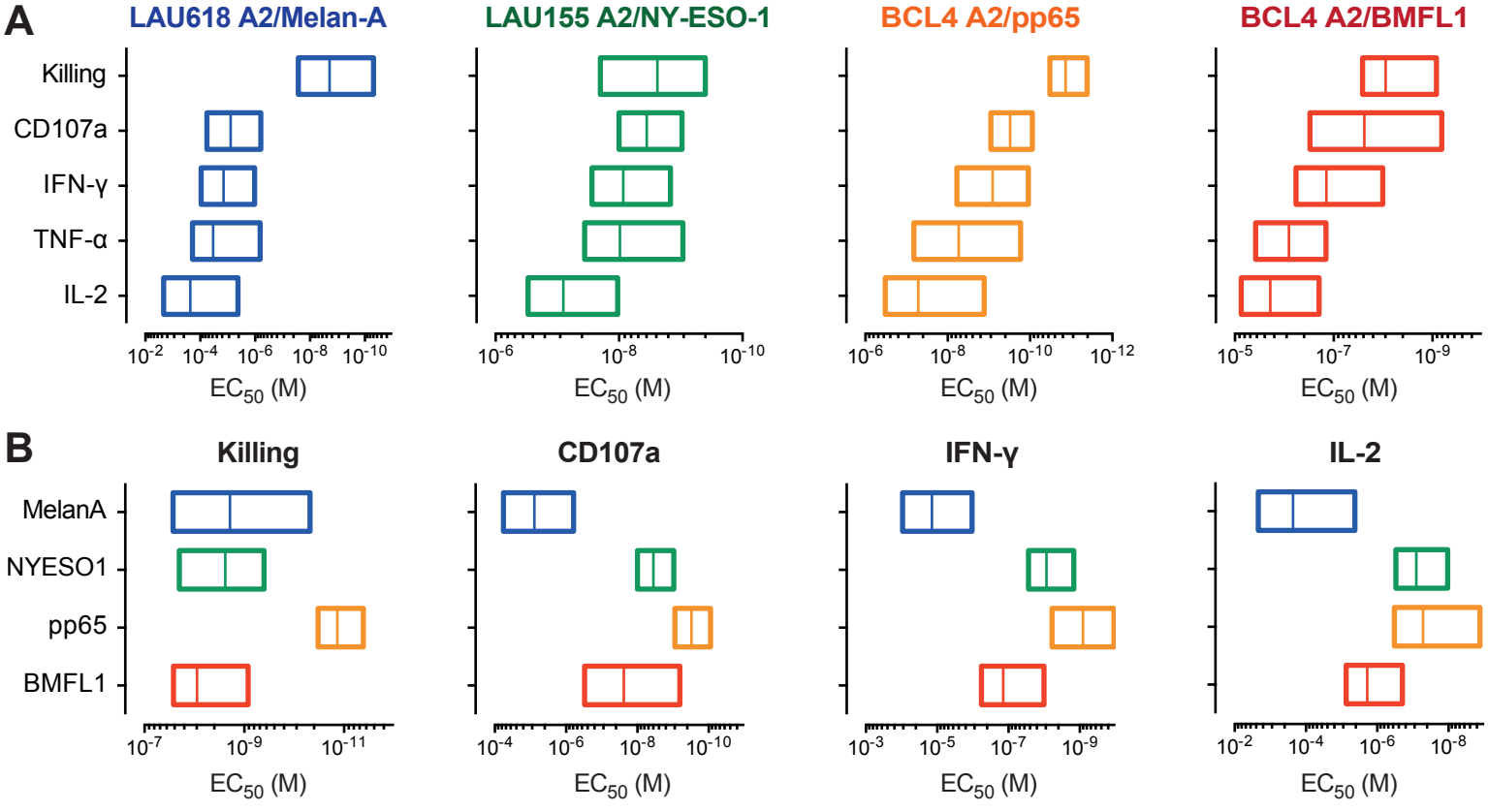

Sup Figure 4 - Allard et al.

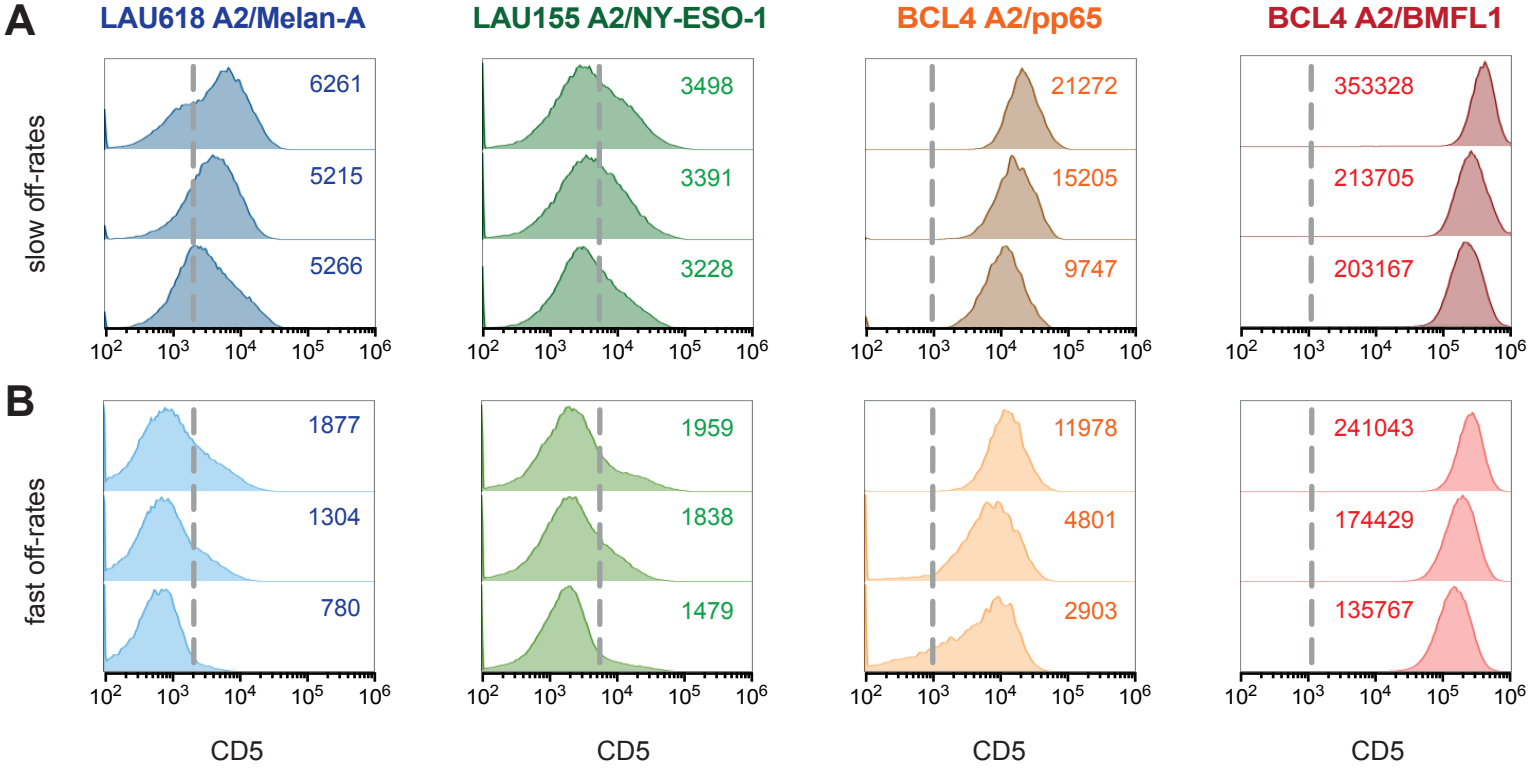

Sup Figure 5 - Allard et al.

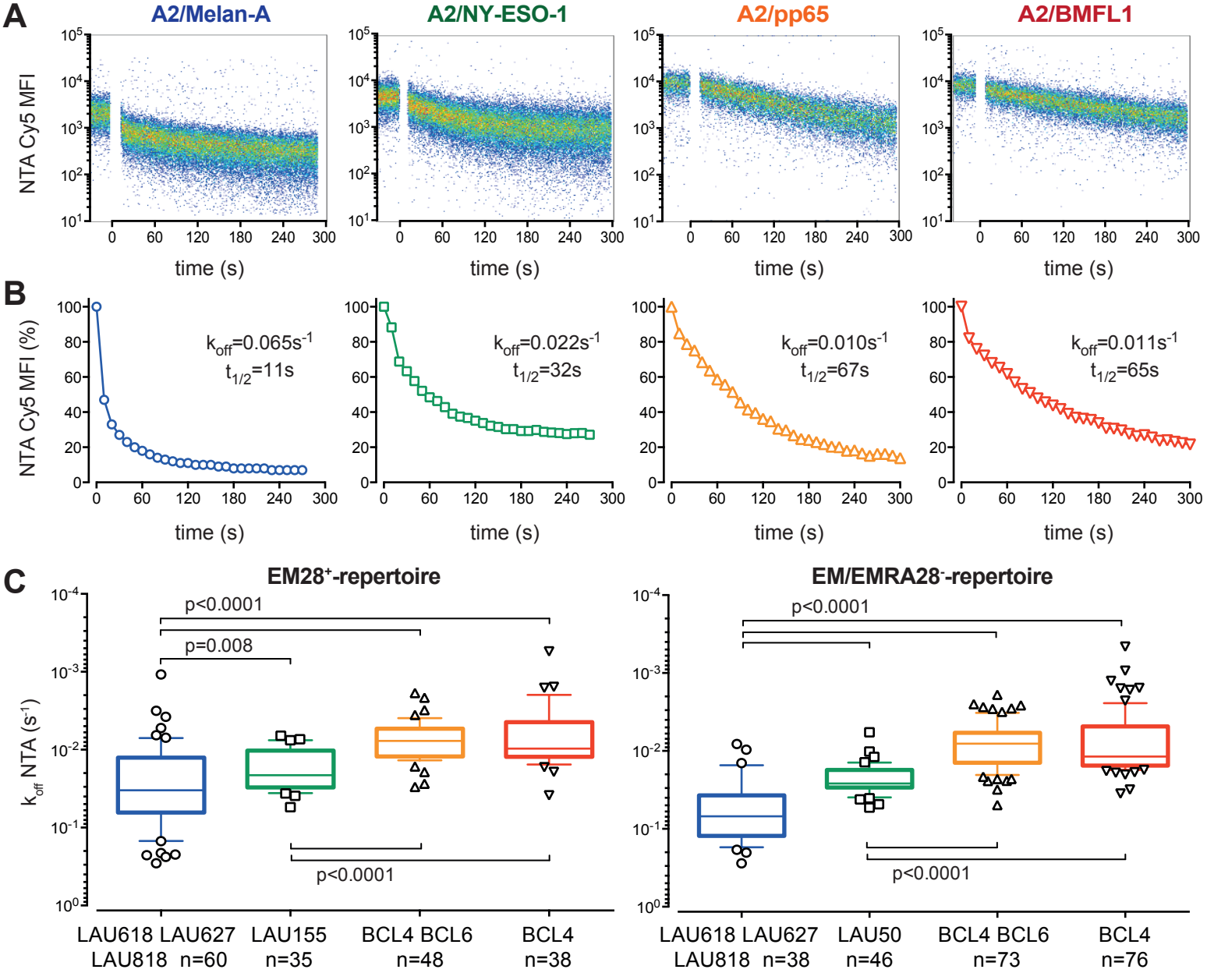

Sup Figure 6 - Allard et al.

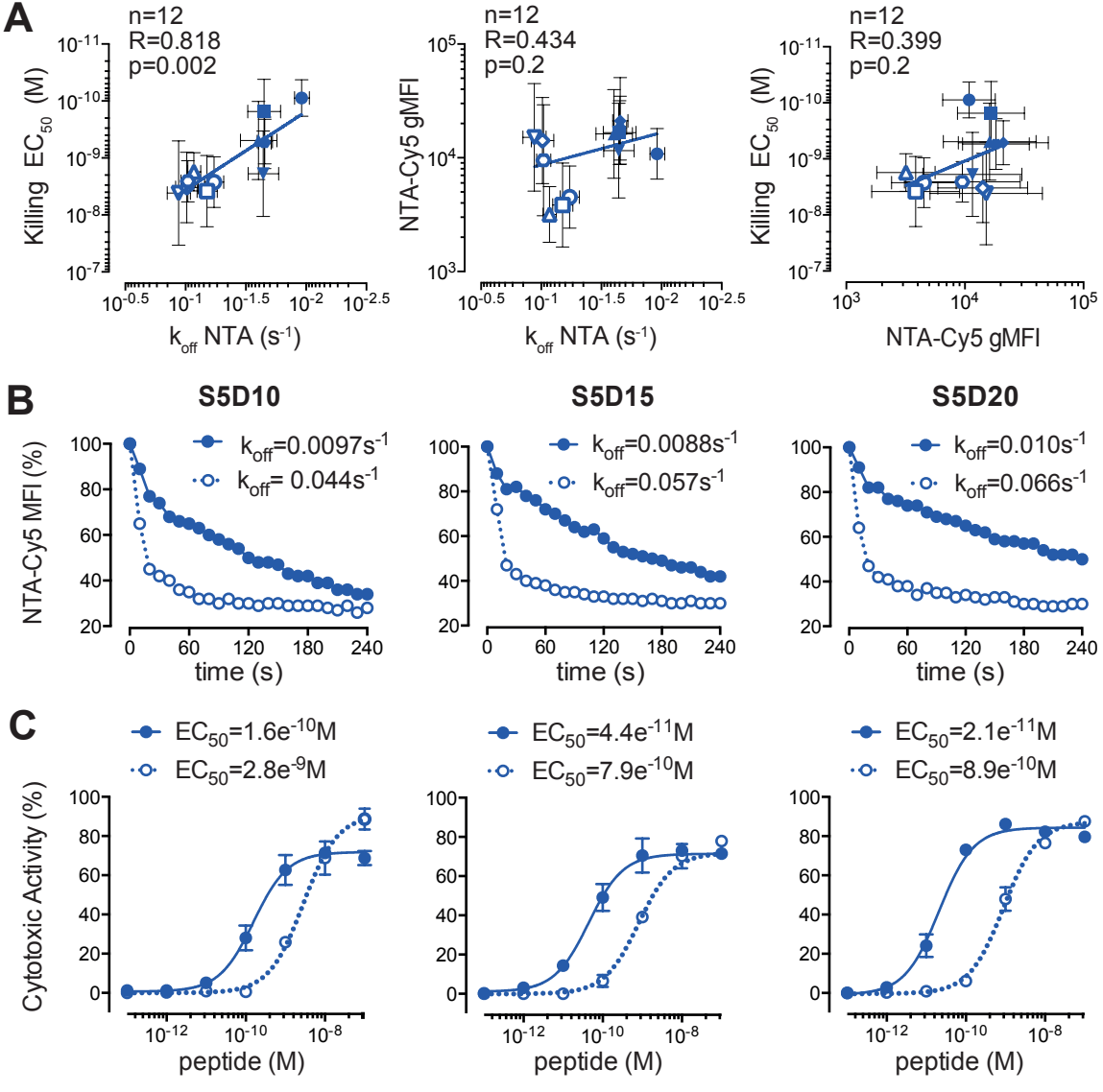

Sup Figure 7 - Allard et al.